6P22R/ Doris
6P01/ Byram
IN-05

AL REPORT

MSFC CRYOSTAT TESTING UNIT

by

d A. Foster, Jr.
Professor

ald M. Jenkins
iate Professor

pared under

No. NAS8-39131-DO32

between

hall Space Flight Center
cs and Space Administration

and

rn University
Experiment Station
rsity, Alabama 36849

pril 1, 1997

ANALYSIS SUPPORTING MSFC CRYOSTAT TESTING UNIT

Winfred A. Foster, Jr. and Rhonald M. Jenkins

ABSTRACT

This report summarizes the results obtained from an analysis of the NASA Marshal Spaceflight Center (MSFC) cryostat testing unit. A finite element model was generated to determine both temperature distribution and stress distribution in the cryostat testing unit for load conditions supplied by MSFC. This report contains the results of that analysis.

ACKNOWLEDGEMENTS

The authors express appreciation to personnel of the George C. Marshall Space Flight Center (MSFC) for their support and assistance in this project. In particular, Mr. David A Shuler whose overall support of this project was an essential factor in its overall success.

TABLE OF CONTENTS

ABSTRACT ii

ACKNOWLEDGMENTS iii

LIST OF FIGURES v

I. Introduction I-1

II. Cryostat Model Description II-1

III. Results III-1

LIST OF FIGURES

Fig. 1. Cryostat finite element model.....III-2
Fig. 2. Cryostat thin shell elements.....III-3
Fig. 3. Cryostat thick shell elements.....III-4
Fig. 4. Cryostat flange elements.....III-5
Fig. 5. Cryostat insulation elements.....III-6
Fig. 6. Outer-surface temperature boundary condition for cold load case.....III-7
Fig. 7. Inner-surface temperature boundary condition for cold load case.....III-8
Fig. 8. Temperature distribution in the cryostat for the cold load case.....III-9
Fig. 9. Normalized pressure on the inner surface.....III-10
Fig. 10. Z-component of displacement for the cold load case.....III-11
Fig. 11. Z-normal stress in the insulation for the cold load case.....III-12
Fig. 12. Max-principle stress in the insulation for the cold load case.....III-13
Fig. 13. Max-shear stress in the insulation for the cold load case.....III-14
Fig. 14. Von-Mises stress in the insulation for the cold load case.....III-15
Fig. 15. Z-normal stress in the thin shell for the cold load case (inner surface).....III-16
Fig. 16. Z-normal stress in the thin shell for the cold load case (outer surface).....III-17
Fig. 17. Max-principle stress in the thin shell for the cold load case (inner surface).....III-18
Fig. 18. Max-principle stress in the thin shell for the cold load case (outer surface).....III-19
Fig. 19. Max-shear stress in the thin shell for the cold load case (inner surface).....III-20
Fig. 20. Max-shear stress in the thin shell for the cold load case (outer surface).....III-21
Fig. 21. Von-Mises stress in the thin shell for the cold load case (inner surface).....III-22
Fig. 22. Von-Mises stress in the thin shell for the cold load case (outer surface).....III-23
Fig. 23. Max-principle stress in the thick shell for the cold load case.....III-24
Fig. 24. Max-shear stress in the thick shell for the cold load case.....III-25
Fig. 25. Von-Mises stress in the thick shell for the cold load case.....III-26
Fig. 26. Max-principle stress in the flange for the cold load case.....III-27
Fig. 27. Max-shear stress in the flange for the cold load case.....III-28
Fig. 28. Von-Mises stress in the flange for the cold load case.....III-29
Fig. 29. Outer-surface temperature boundary condition for hot load case.....III-30
Fig. 30. Temperature distribution in the cryostat for the hot load case.....III-31
Fig. 31. Z-component of displacement for the hot load case.....III-32
Fig. 32. Z-normal stress in the insulation for the hot load case.....III-33
Fig. 33. Max-principle stress in the insulation for the hot load case.....III-34
Fig. 34. Max-shear stress in the insulation for the hot load case.....III-35
Fig. 35. Von-Mises stress in the insulation for the hot load case.....III-36
Fig. 36. Z-normal stress in the thin shell for the hot load case (inner surface).....III-37
Fig. 37. Z-normal stress in the thin shell for the hot load case (outer surface).....III-38
Fig. 38. Max-principle stress in the thin shell for the hot load case (inner surface).....III-39
Fig. 39. Max-principle stress in the thin shell for the hot load case (outer surface).....III-40
Fig. 40. Max-shear stress in the thin shell for the hot load case (inner surface).....III-41
Fig. 41. Max-shear stress in the thin shell for the hot load case (outer surface).....III-42
Fig. 42. Von-Mises stress in the thin shell for the hot load case (inner surface).....III-43

LIST OF FIGURES (Continued)

Fig. 43. Von-Mises stress in the thin shell for the hot load case (outer surface).....III-44
Fig. 44. Max-principle stress in the thick shell for the hot load case.....III-45
Fig. 45. Max-shear stress in the thick shell for the hot load case.....III-46
Fig. 46. Von-Mises stress in the thick shell for the hot load case.....III-47
Fig. 47. Max-principle stress in the flange f or the hot load case.....III-48
Fig. 48. Max-shear stress in the flange for the hot load case.....III-49
Fig. 49. Von-Mises stress in the flange for the hot load case.....III-50

I. Introduction

The goal of this project was to develop a model of the MSFC cryostat test facility, for the purpose of determining the stress distribution in the cryostat under typical test conditions. Of particular interest was the stress state at the bond-line between the internal insulation and the Al-Li tank wall. The analysis used a finite element model of a quarter section of the cryostat. The model is used to predict the temperature distribution within the cryostat using thermal loads which would be typical during a test. The calculated temperature distribution is then used to impose a thermal load on the cryostat in conjunction with typical test pressure loads. Material property variation with temperature for both thermal and mechanical properties is accounted for based on data supplied by MSFC.

The finite element analysis was non-linear in that the material properties were temperature dependent and that large deformations were accounted for in the static analysis. The large deformation solution was used because the bending deformations in the thin shell portion of the tank were large compared to the thickness.

This report contains a brief discussion of the finite element model and results for various deformation and stress components.

II. Cryostat Model Description

Model Description

A one quarter model of the cryostat was constructed to take advantage of rotational symmetry. Because of the basic circular shape of the cryostat a cylindrical coordinate system was used for defining the model geometry, the constraints and the load conditions. The intent of the analysis was to determine the stress distribution within the cryostat and in particular the bond line stresses between the insulation and the tank wall. The model is separated into three sections: an Aluminum-Lithium fuel tank shell, a section of Aluminum flange and a layer of insulation attached to the inner surface of the tank wall. Figures 1 thru 5 show the finite element model of the cryostat.

Fuel Tank Shell:

The fuel tank shell section is a dome with a radius of curvature of 80". The radius of the dome is 16.125" with a bolt circle at 15.57" radius. The model stops at this bolt circle. The thickness of the tank wall is .045" from the center to a radius of 10.205". The wall thickness gradually increases to .19" at a radius of 15.0". At this point the tank wall flattens to meet with the test fixture.

The section of the tank wall that is .045" thickness is modeled with CQUAD4 2-D shell elements. In the region where the tank wall begins to expand in thickness the model transitions with a circumferential ring of 3-D CPENTA (pentahedron) elements to 3-D CHEXA (hexadron) elements out to the bolt circle. There are two elements through the thickness.

Insulation:

The insulation is attached to the interior surface of the tank wall and is 1.0" thick. The insulation extends from the radial center to a radius of 15.0". At this point the insulation contacts the aluminum test flange. The insulation is modeled with CHEXA elements and has three elements through the thickness.

Aluminum Test Flange:

In order for the cryostat to be tested it must be attached to a test flange, a small portion of this test flange has been included for model continuity. The test flange section is also 1.0" thick and is attached to the interior face of the tank wall on the outermost flat section of the tank wall. The radially inward face of the flange attaches to the radially outward face of the insulation. The flange extends from a radius of 15.0" to a radius of 15.57". The entire flange is modeled with CHEXA elements. The flange is modeled with three elements radially and three elements through the thickness in order to match both the fuel tank and the insulation.

Material Property Description

Fuel Tank Wall:

Aluminum-Lithium alloy properties as supplied by MSFC were utilized for the tank wall. Nominal values are: the elastic modulus (E) being 1.1097897E7 psi, Poisson's Ration (ν) was 0.329, the modulus of rigidity (G) was 4.1740392E6 psi, the weight density (ρ) was 0.101 lbf/in^3, the coefficient of thermal Expansion (α) was 1.28 E-5 in/in·°F at the reference temperature of 70°F. Temperature dependent properties obtained from MSFC were incorporated into the final analysis of the cryostat Al-Li tank wall for both the thermal and mechanical analysis.

Insulation:

The model utilized Cemafoam as the insulation material. Material property data documents were provided by MSFC. Nominal values are; for the elastic modulus (E) was 1.59E4 psi, Poisson's Ration (ν) was 0.3, the modulus of rigidity (G) was 6.115E3 psi, the weight density (ρ) was 0.01 lbf/in^3, the coefficient of thermal expansion (alpha) was 1.944E-8 in/in·°F at the reference temperature of 70°F. Once again, temperature dependent material properties obtained from MSFC were used in the final analysis of the cryostat insulation. For both the thermal and mechanical analysis.

Aluminum Flange:

The flange section of the model utilized Al 2219 as per Mil-HDBK 5E. The elastic modulus (E) was 1.05E7 psi, Poisson's Ration (ν) was 0.33, the modulus of rigidity (G) was 4.0E6 psi, the weight density (ρ) was 0.103 lbf/in^3, the coefficient of thermal expansion (alpha) was 1.23E-5 in/in·°F at the reference temperature of 70°F.

Boundary Conditions

Two sets of boundary conditions were applied to the entire model for all loading cases. The first set provided symmetry at the two "cut" faces of the ninety degree section of the cryostat model. The second set provided for simulation of a rigid, bolted interface between the outer, flattened section of the cryostat and the test flange.

Symmetry Boundary Conditions:

As previously mentioned the model is a ninety degree section of a circular structure in which all geometry, boundary conditions and loads are defined in a cylindrical coordinate system. Therefore in order to provide symmetry at the "cut" faces the "Theta", out of plane displacement and the two out of plane rotational degrees of freedom for all nodes on the faces were constrained to zero. Additionally at the radial center of the model the "radial", horizontal, in-plane displacement degree of freedom for nodes at this location were constrained to zero as well.

Bolted Boundary Condition:

The radial outer edge of the model is at 15.57". All nodes along this outer perimeter were constrained in all displacement and rotational degrees of freedom.

Loading Environment

Four separate loads, two temperature loads and two pressure loads have been combined into two load cases.

Load Case 1 :

This load case simulates the loading conditions that would be experienced when the tank contains a pressurized cryogenic liquid. All nodes on the inner surface of the insulation layer, interior of the fuel tank, have their temperatures constrained to -320°F while all nodes on the outer surface of the fuel tank wall, exterior of the fuel tank, have their temperatures constrained to +70°F. In addition the outer constraint, +70°F, also continues up the outer perimeter of the model onto the outer surface of the flange. All nodes on the top surface of the flange are left unconstrained in order to allow a temperature gradient to develop across the flange thickness. In addition to the thermal load acting on the structure, an internal pressure of 45 psi is also present.

Load Case 2:

This load case simulates the worst case temperature gradient with a minimum internal pressure. This would simulate the tank being heated after most of the cryogenic liquid has been expelled from the tank. All nodes on the inner surface of the insulation layer, interior of the fuel tank, have their temperatures constrained to -320°F while all nodes on the outer surface of the fuel tank wall, exterior of the fuel tank, have their temperatures constrained to +350°F. In addition the outer constraint, +350°F, also continues up the outer perimeter of the model onto the outer surface of the flange. All nodes on the top surface of the flange are again left unconstrained in order to allow a temperature gradient to develop across the flange thickness. The internal pressure is assumed to be 5 psi.

III. Results and Conclusions

The results obtained from this analysis consist of the temperature and stress distributions within the Cryostat test article. The results presented are for two load cases. The first, or cold case, is defined by an inside insulation wall temperature of -320 °F , an outside tank wall temperature of 70 °F and an internal pressure of 45 psi. The second, or hot case, is define by an inside insulation wall temperature of -320 °F, an outside tank wall temperature of 350 °F and an internal pressure of 5 psi.

The resulting temperature distribution within the cryostat for the cold case is shown in Figure 8. The deflections in the z-direction (axis of symmetry direction) due to the combined thermal and mechanical loads are shown in Figure 10. Contour plots for the z-normal stress component, the max-principle stress, the max-shear stress and the Von-Mises effective stress in the insulation material are shown in Figures 11 thru 14, respectively. Figures 15 thru 22 show contour plots of the z-normal stress, the max-principle stress, the max-shear stress and the Von-Mises effective stress for the thin-walled (2-D model) portion of the cryostat wall. There are two plots for each of the stresses shown, one for the inner surface and one for the outer surface. This is necessary to show the effects of bending in this portion of the shell. Figures 23 thru 25 show the max-principle stress, the max-shear stress and the Von-Mises effective stress for the thick-walled (3-D model) portion of the cryostat tank wall. Figures 26 thru 28 show these same components for the flange.

The resulting temperature distribution within the cryostat for the hot case is shown in Figure 30. The deflections in the z-direction (axis of symmetry direction) due to the combined thermal and mechanical loads are shown in Figure 31. Contour plots for the z-normal stress component, the max-principle stress, the max-shear stress and the Von-Mises effective stress in the insulation material are shown in Figures 32 thru 35, respectively. Figures 36 thru 43 show contour plots of the z-normal stress, the max-principle stress, the max-shear stress and the Von-Mises effective stress for the thin-walled (2-D model) portion of the cryostat wall. There are two plots for each of the stresses shown, one for the inner surface and one for the outer surface. This is necessary to show the effects of bending in this portion of the shell. Figures 44 thru 46 show the max-principle stress, the max-shear stress and the Von-Mises effective stress for the thick-walled (3-D model) portion of the cryostat tank wall. Figures 47 thru 49 show these same components for the flange.

The results do not appear to show any unusually high stresses or deflections for the load cases analyzed. Since there were no failure criteria specifications given for the analysis, no further definitive conclusions can be reached as to the structural integrity of the test unit. The models developed for the analysis should be suitable for applications to future changes in insulation and tank materials and therefore do provide a useful basis for further analysis.

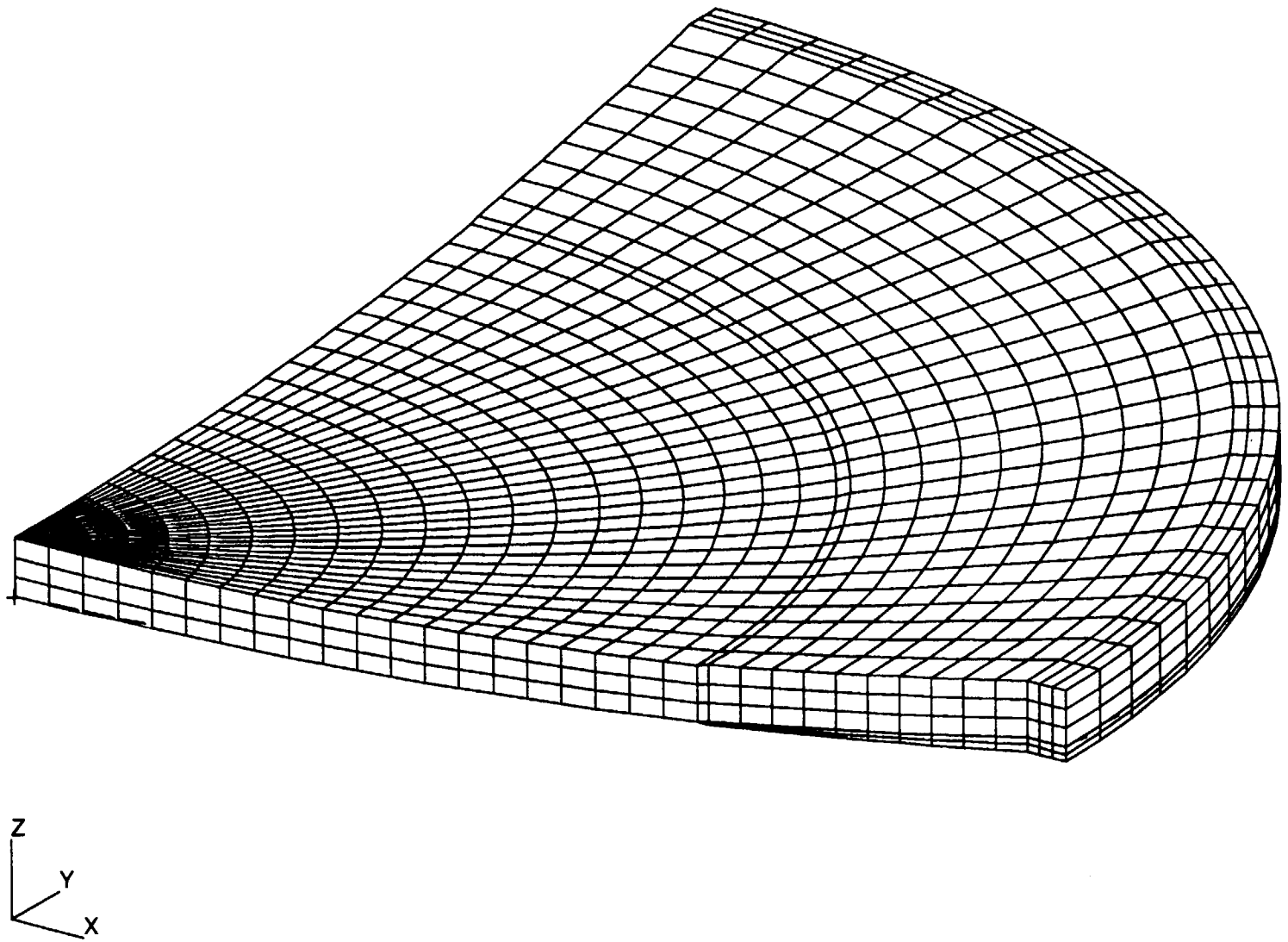

Fig. 1. Cryostat finite element model.

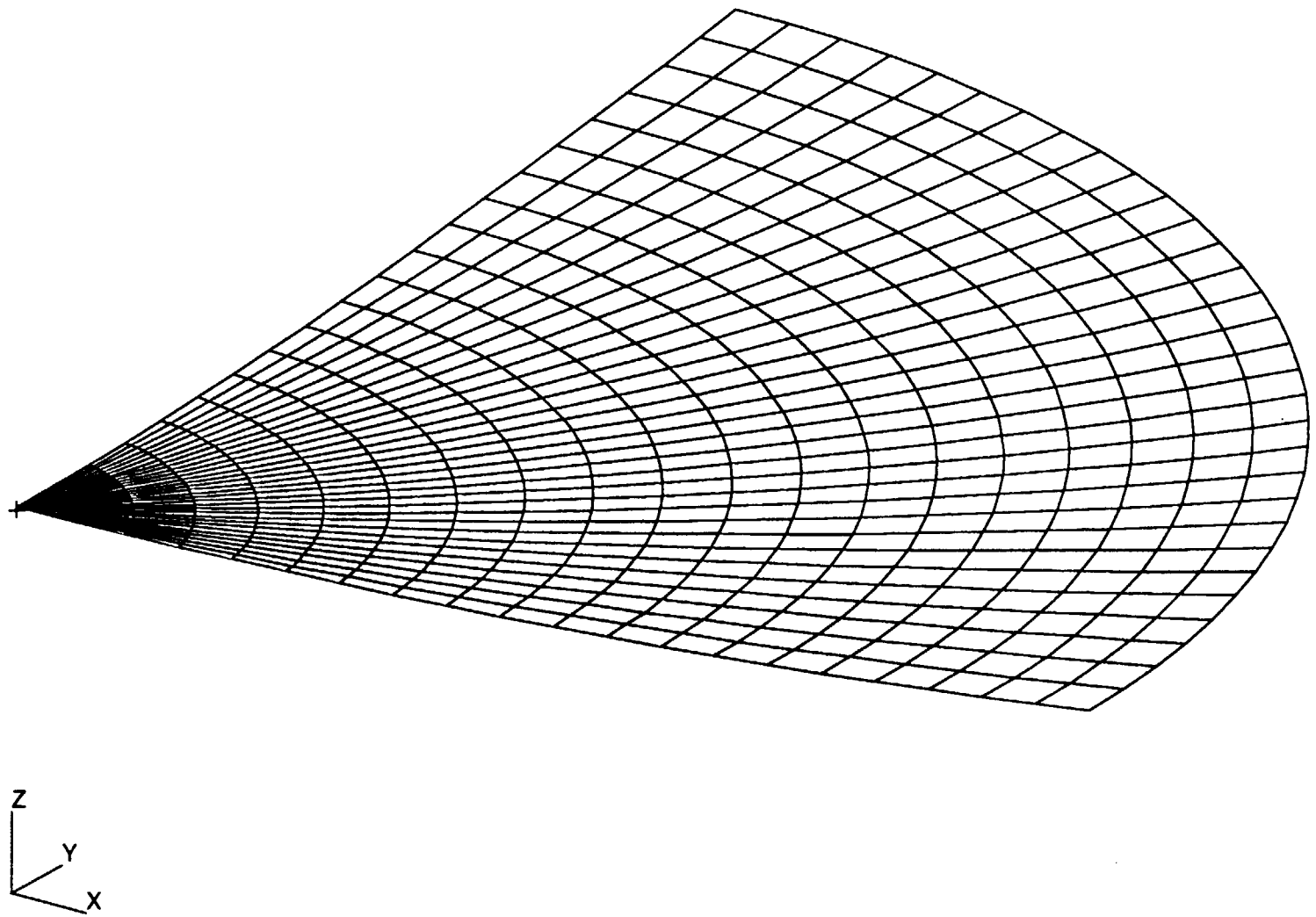

Fig. 2. Cryostat thin shell elements.

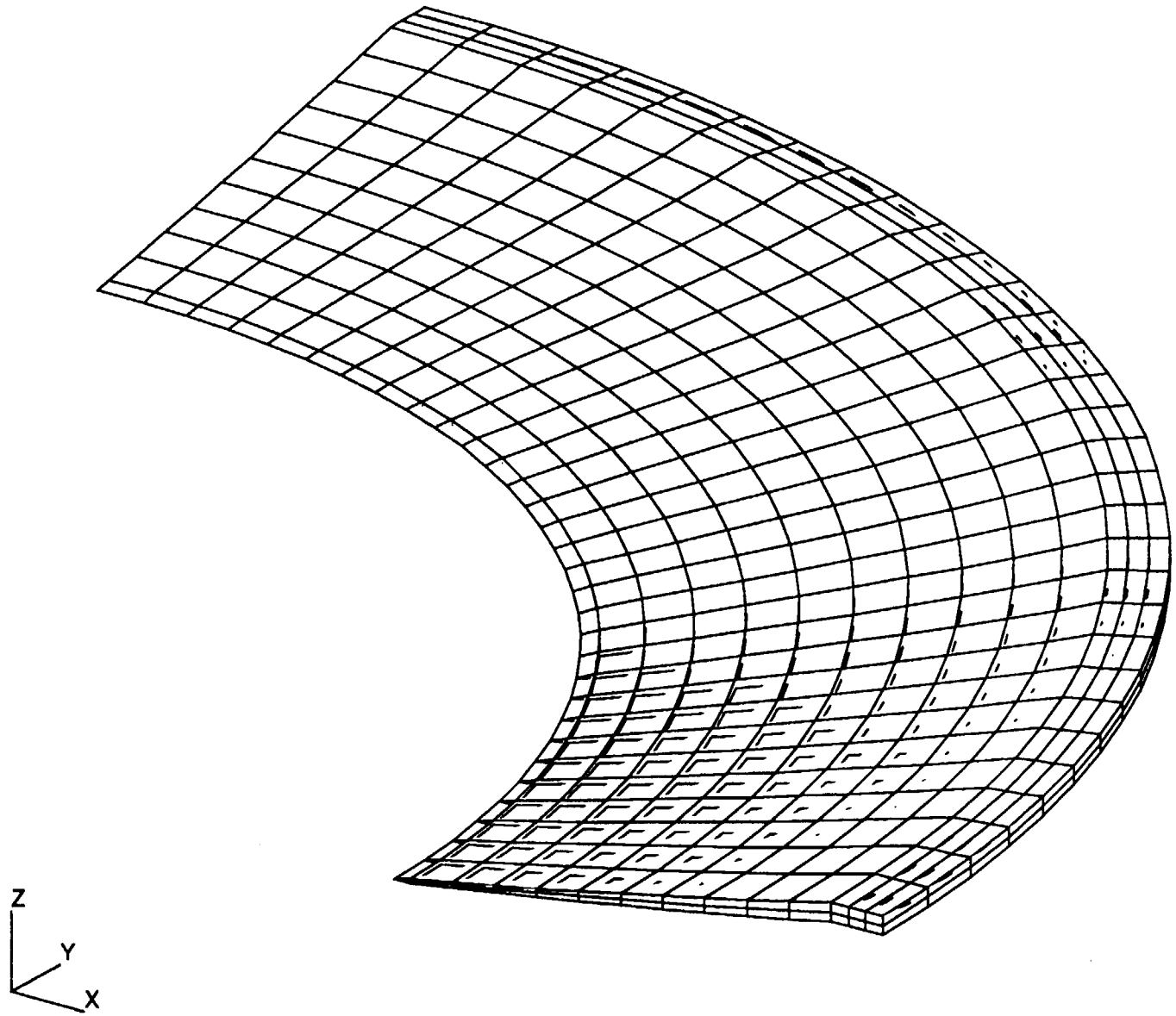

Fig. 3. Cryostat thick shell elements.

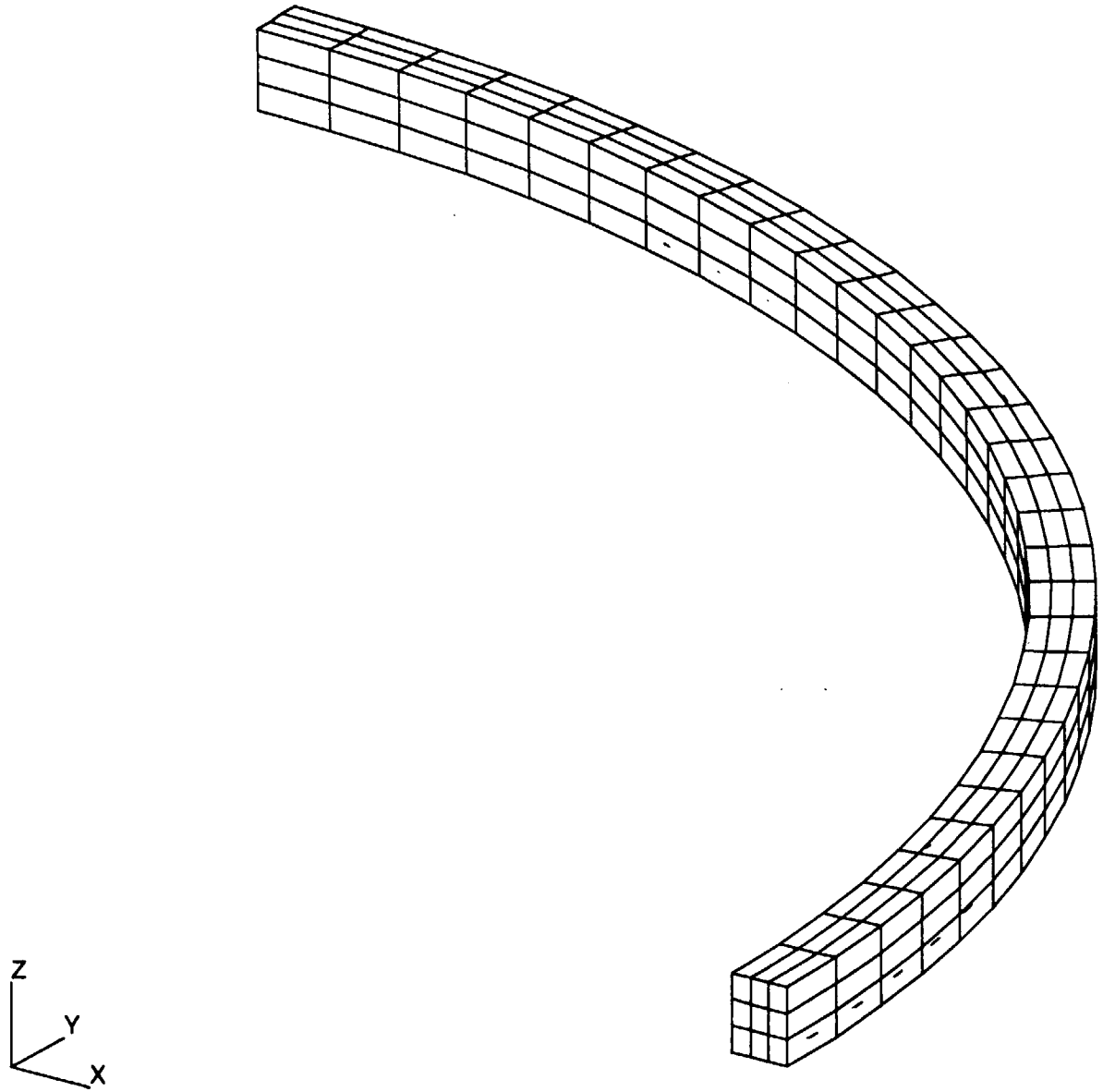

Fig. 4. Cryostat flange elements.

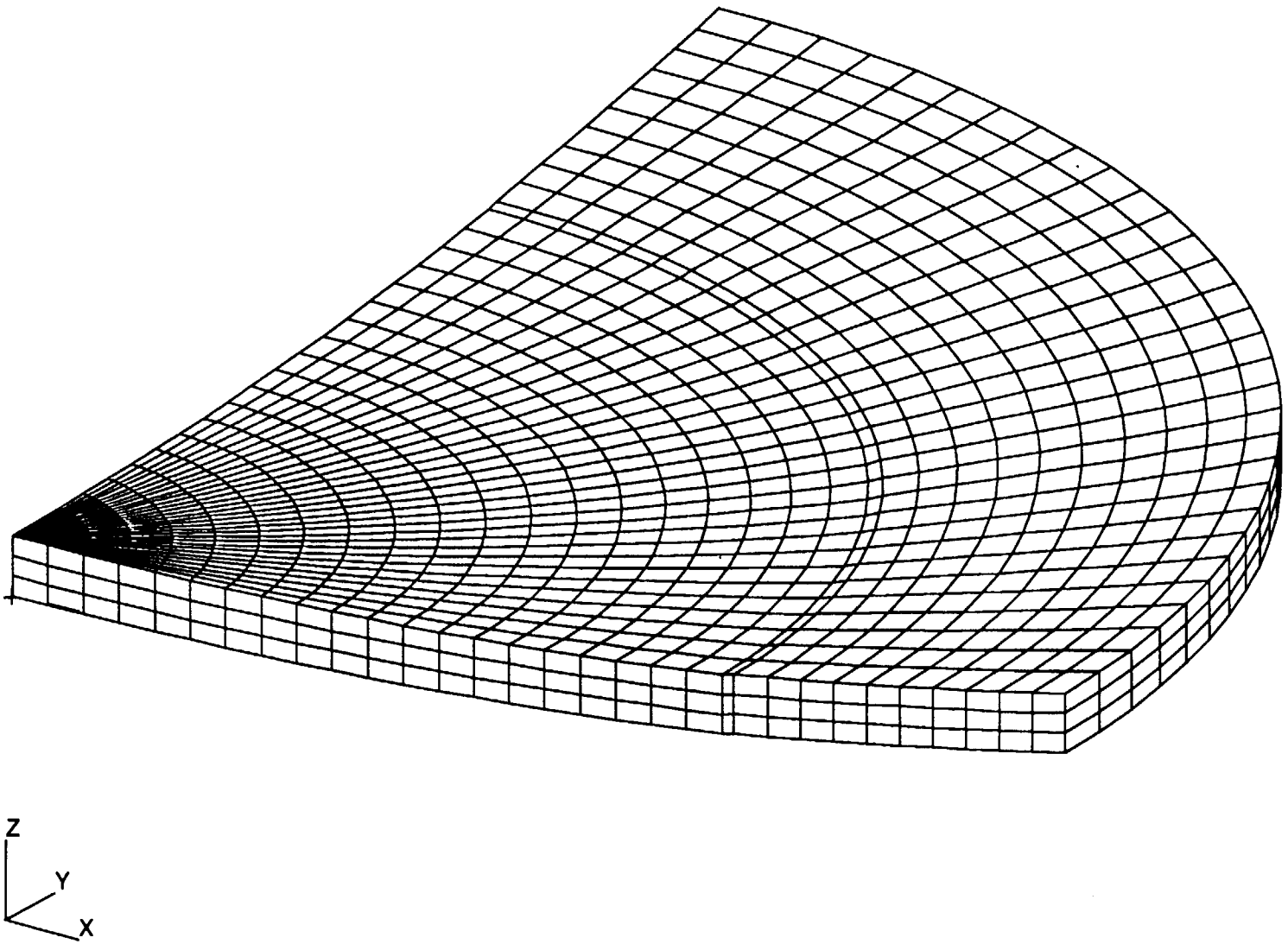

Fig. 5. Cryostat insulation elements.

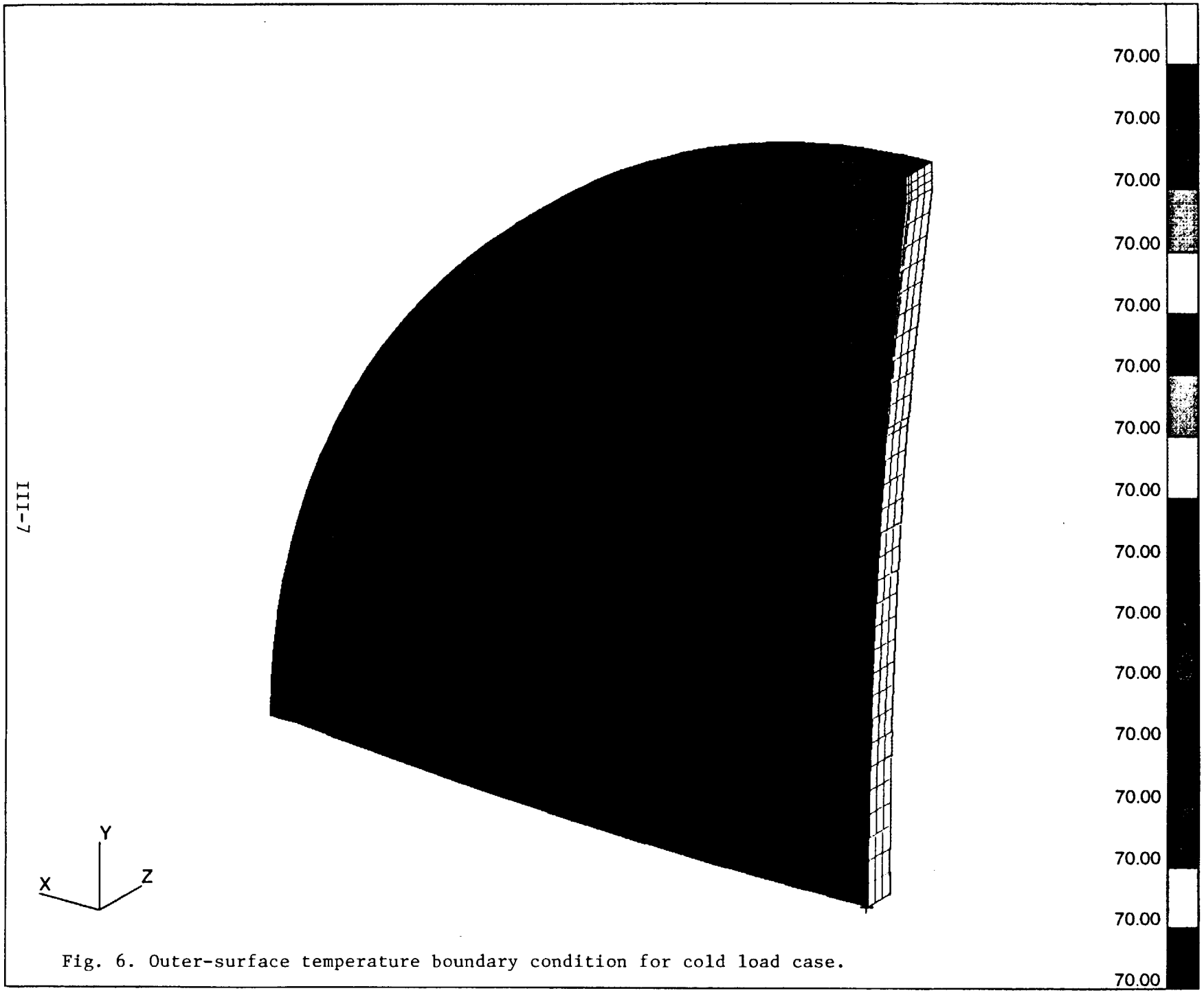

Fig. 6. Outer-surface temperature boundary condition for cold load case.

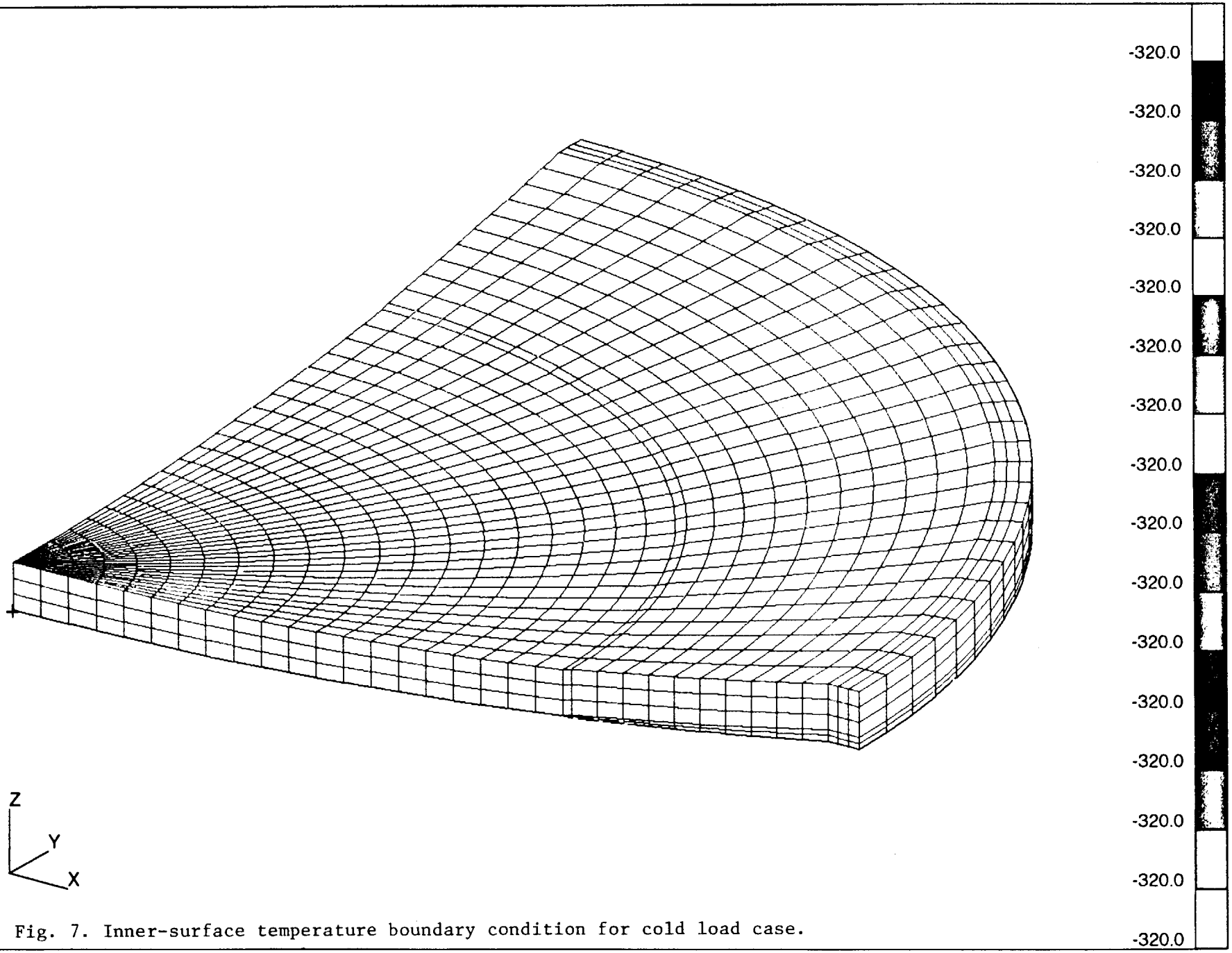

Fig. 7. Inner-surface temperature boundary condition for cold load case.

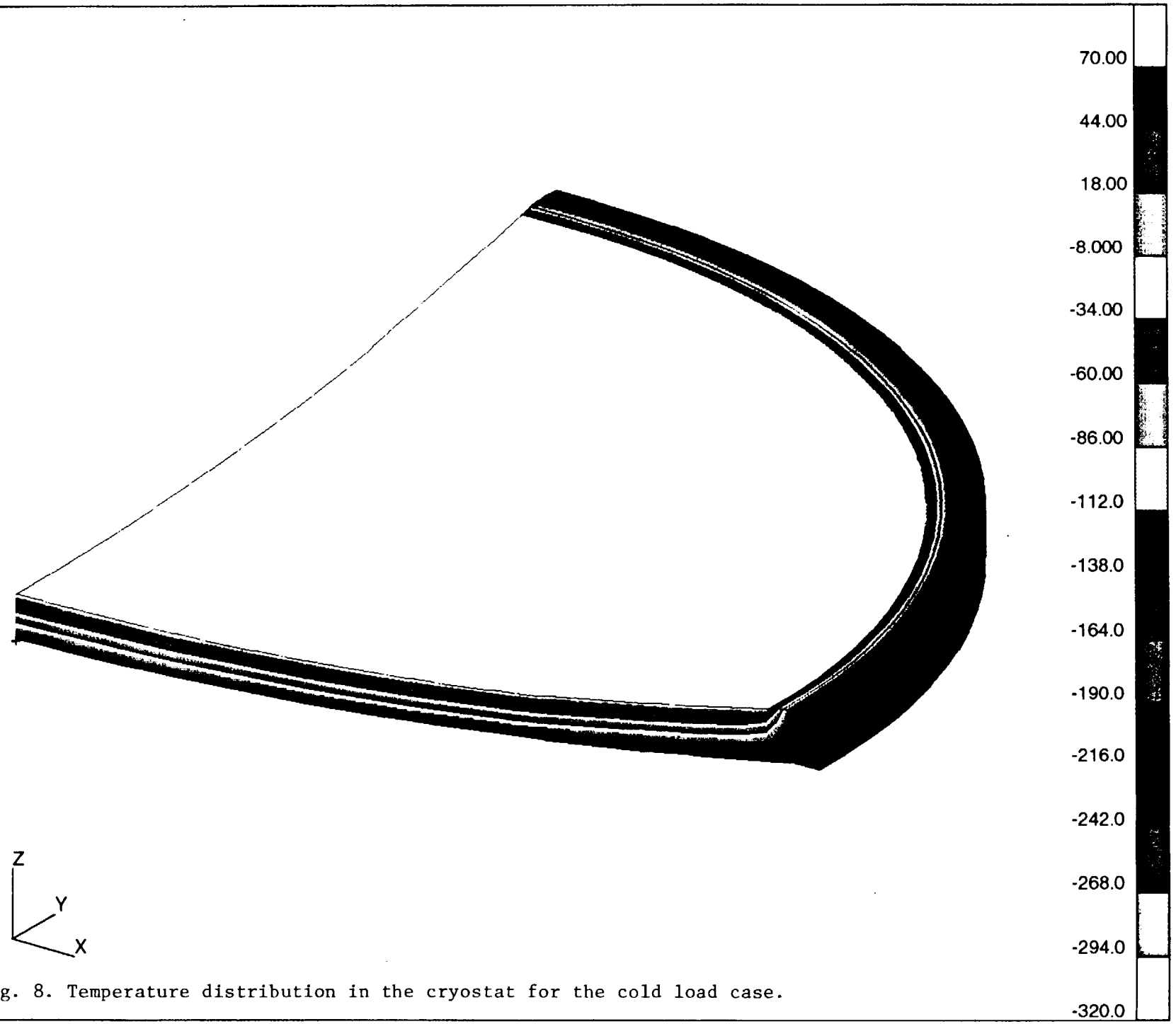

Fig. 8. Temperature distribution in the cryostat for the cold load case.

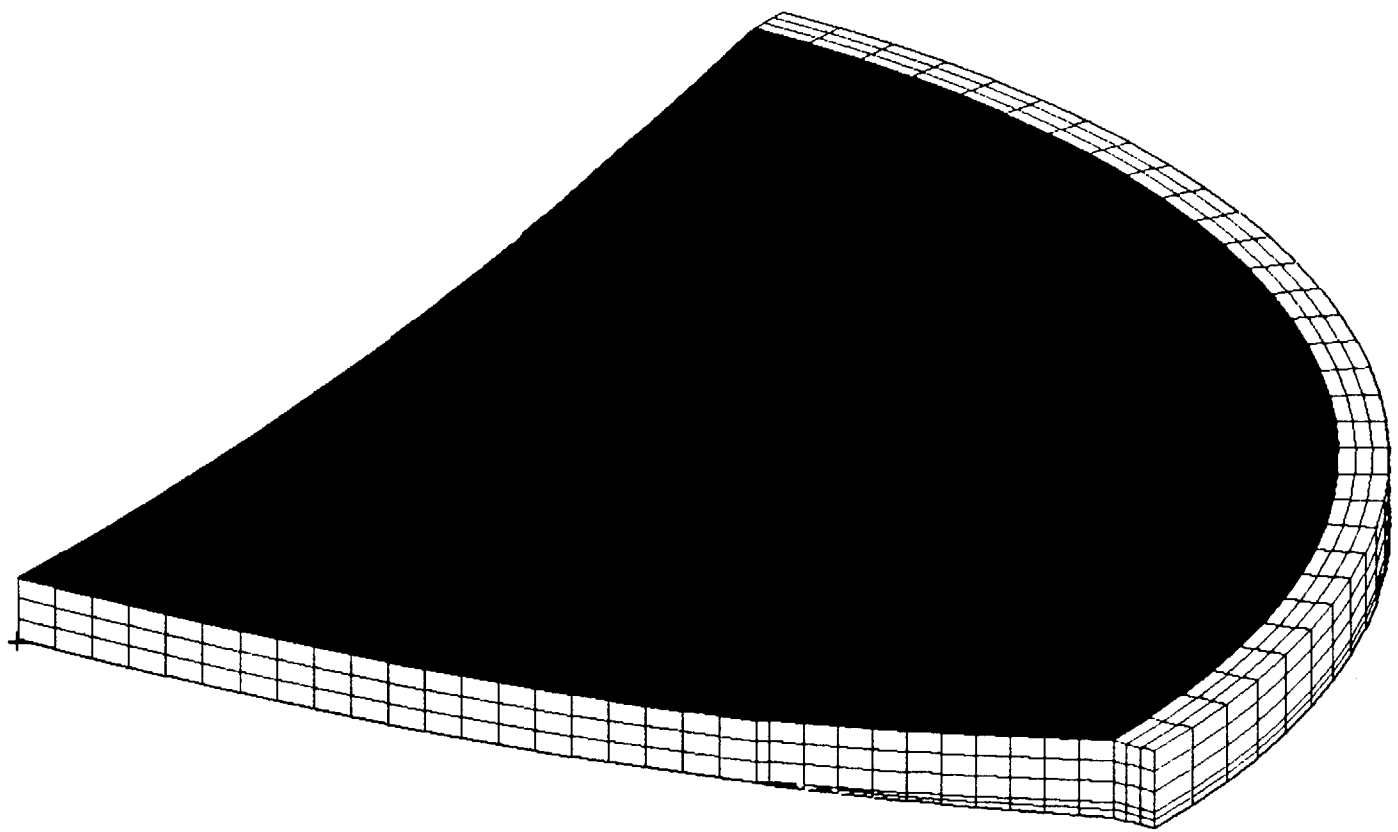

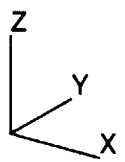

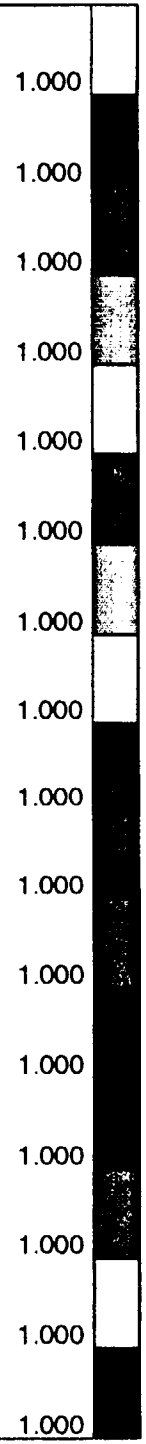

Fig. 9. Normalized pressure on the inner surface.

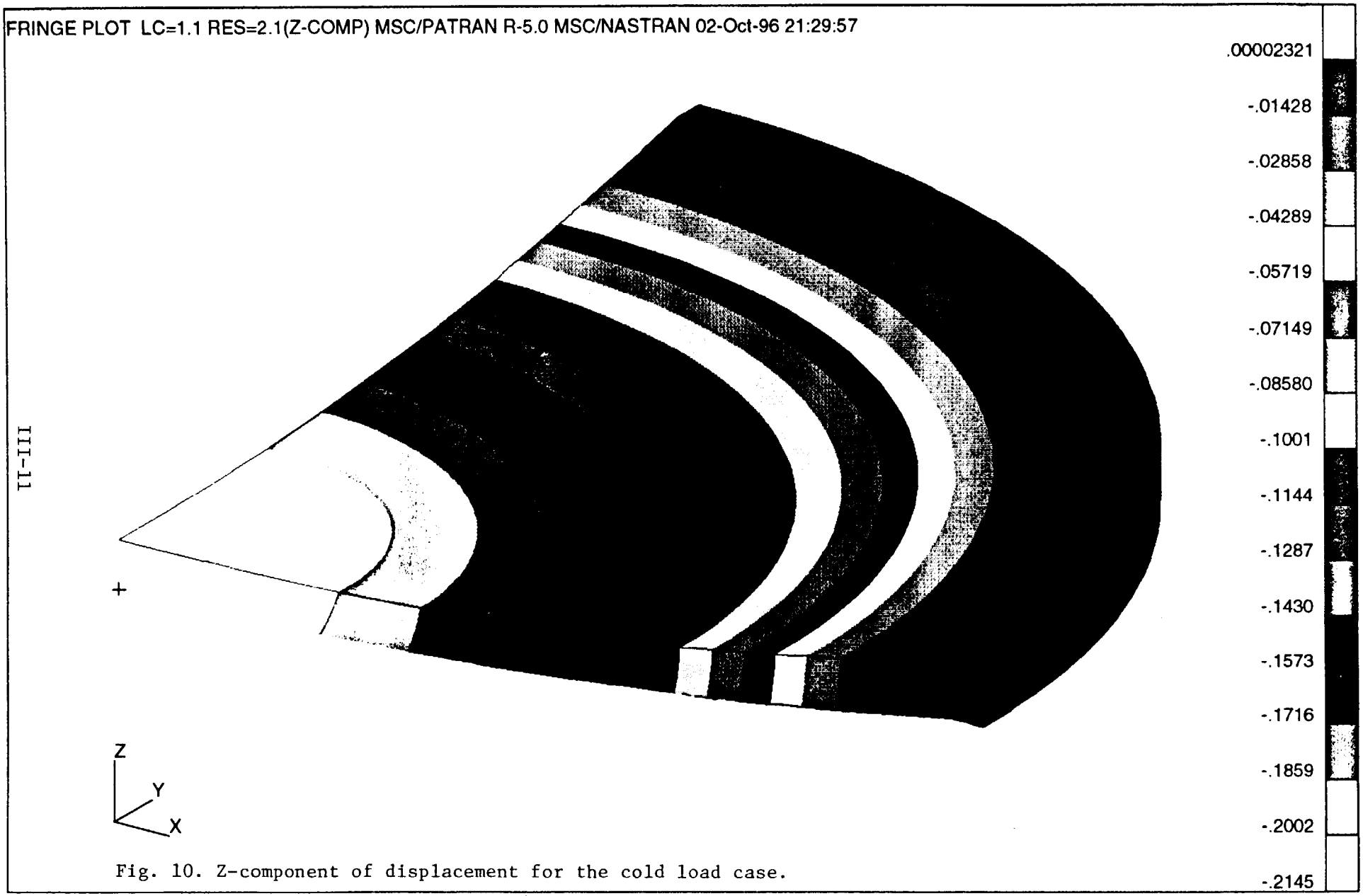

Fig. 10. Z-component of displacement for the cold load case.

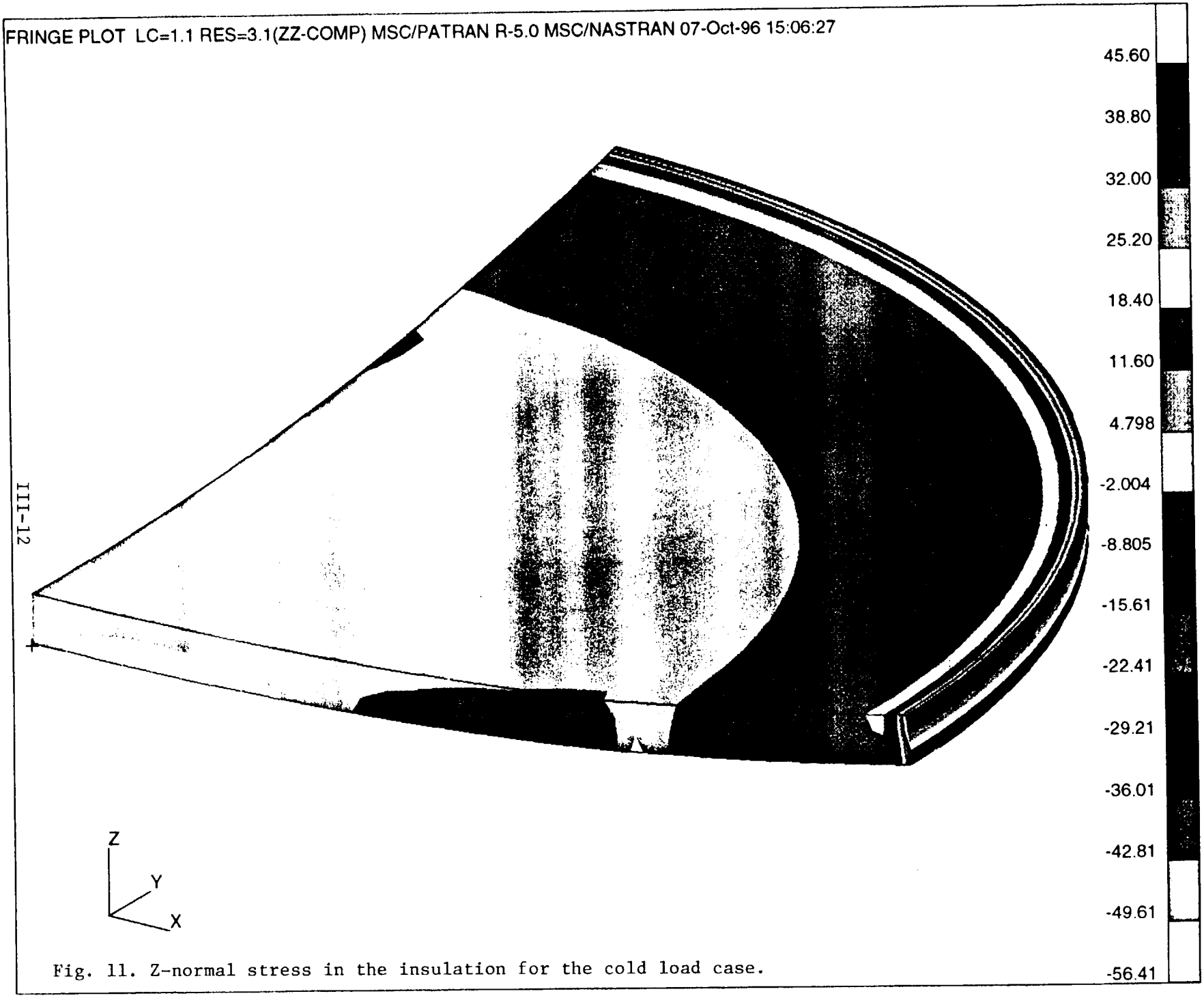

Fig. 11. Z-normal stress in the insulation for the cold load case.

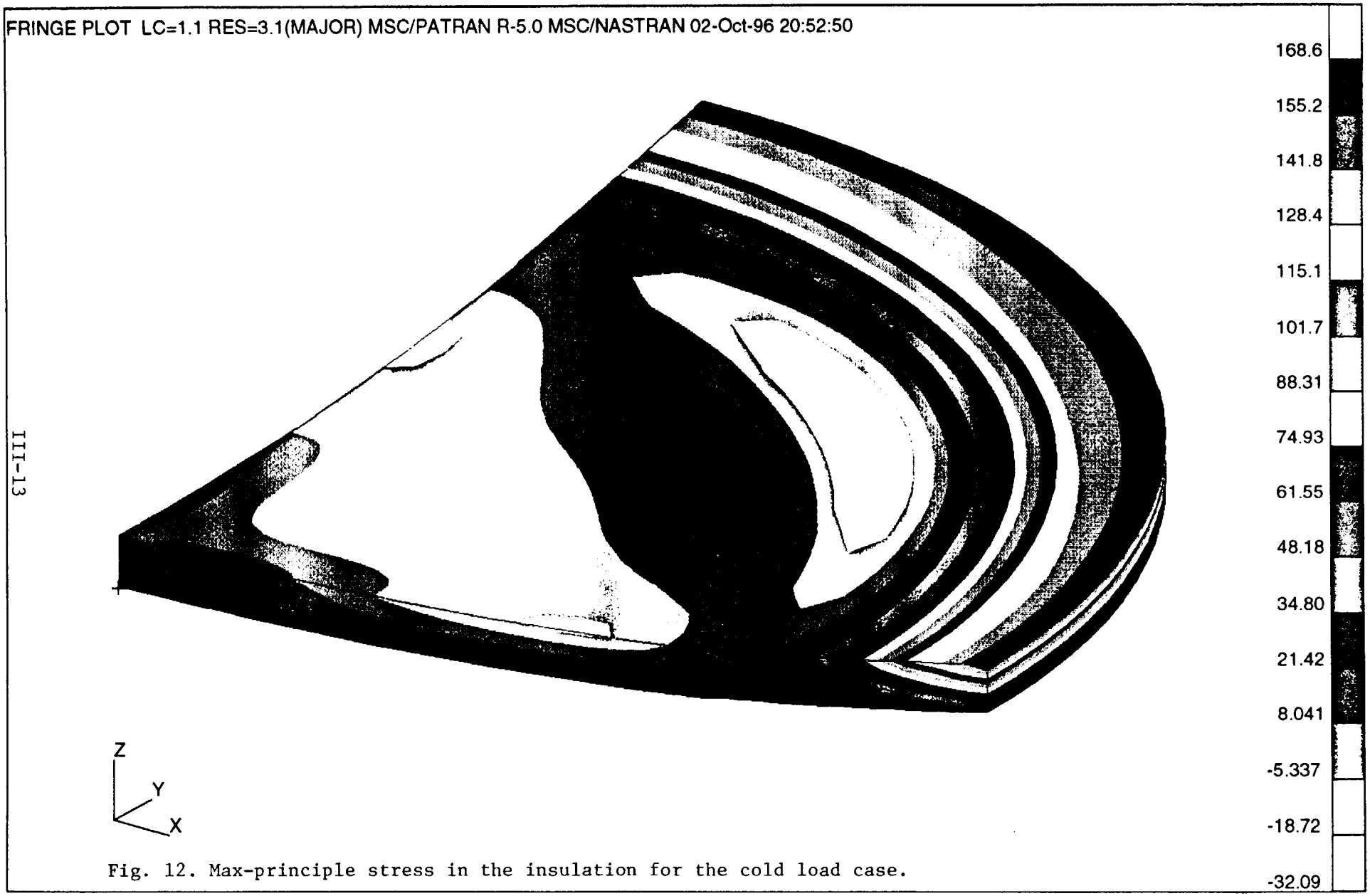

Fig. 12. Max-principle stress in the insulation for the cold load case.

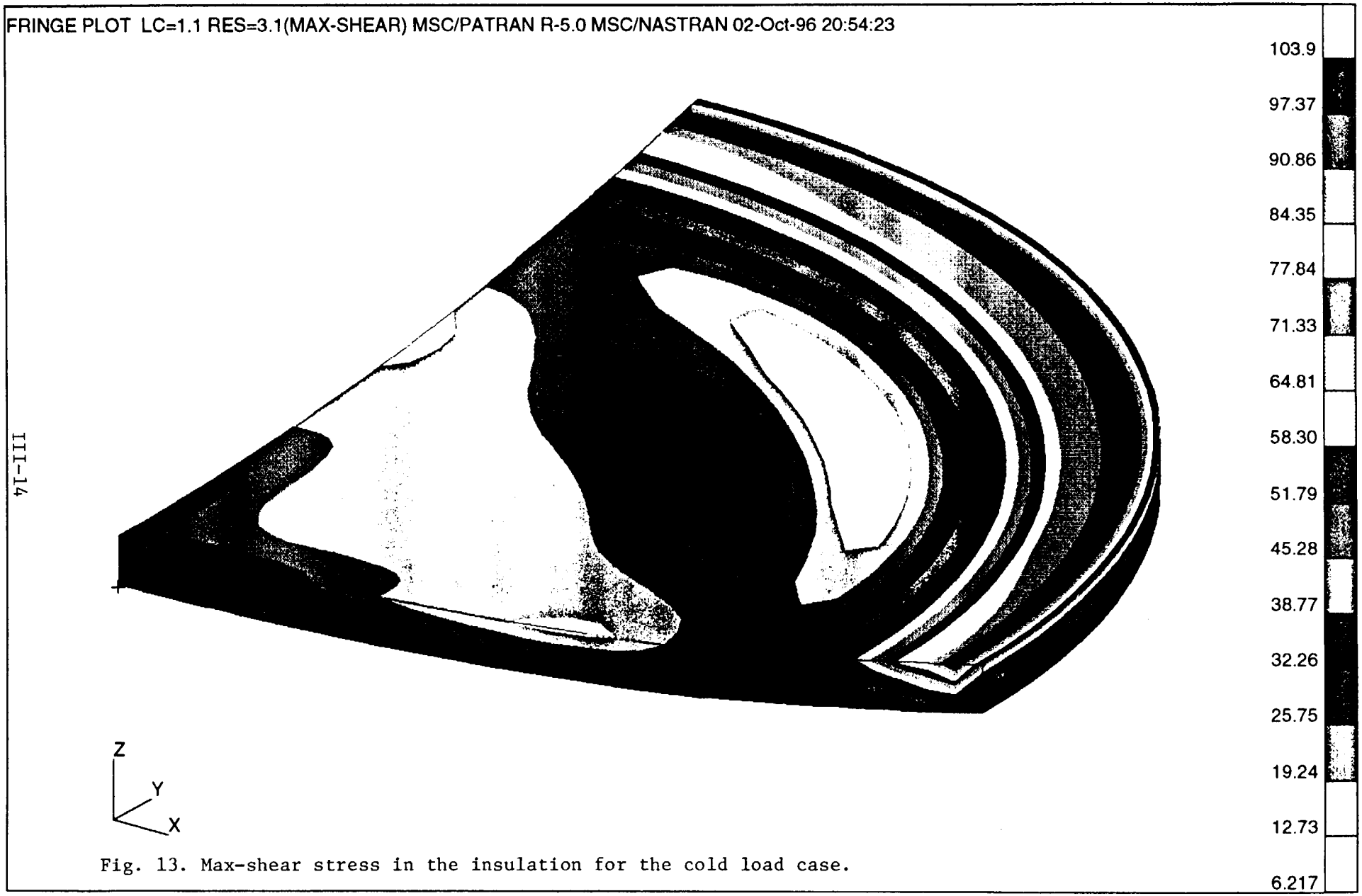

Fig. 13. Max-shear stress in the insulation for the cold load case.

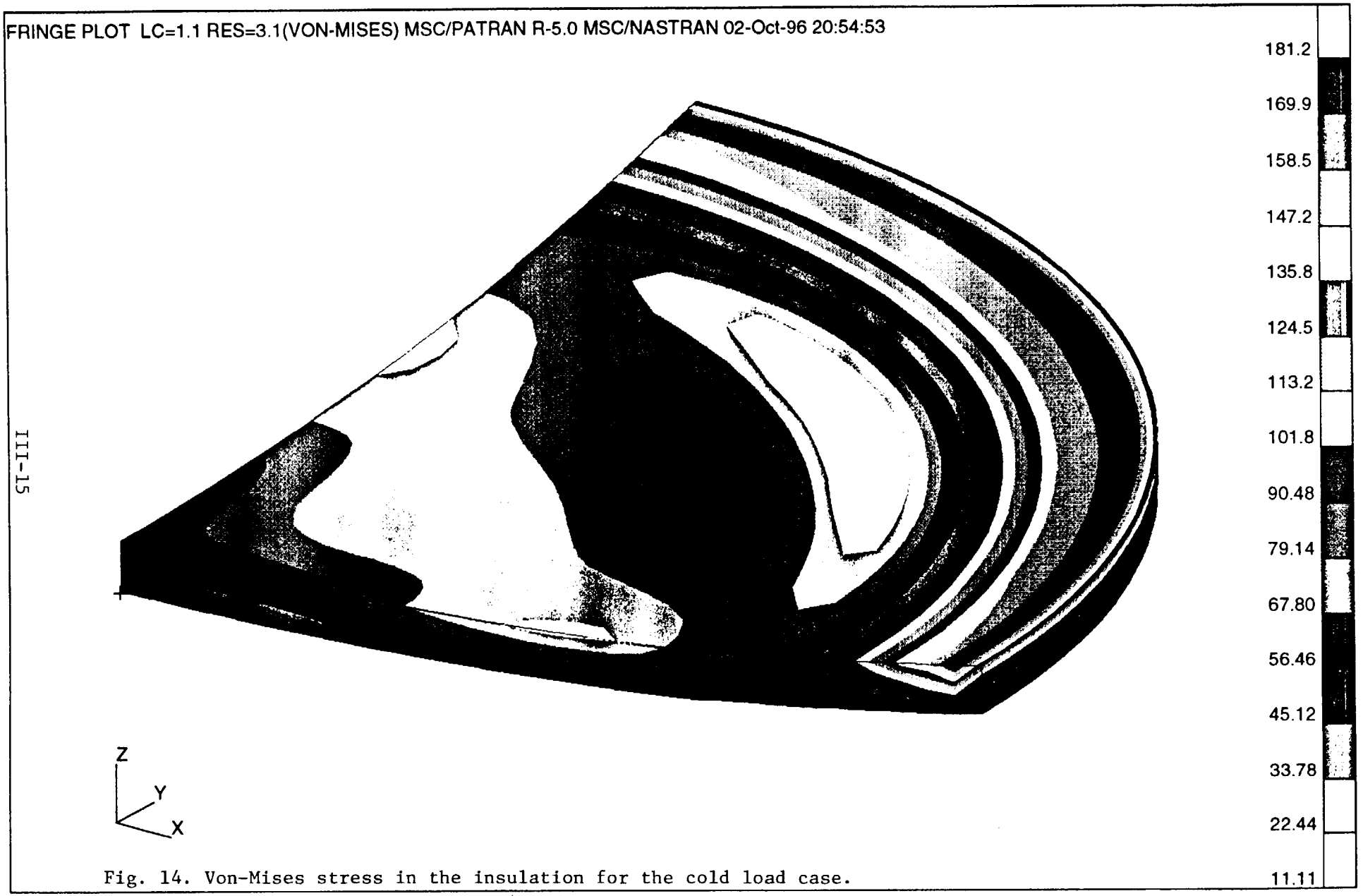

Fig. 14. Von-Mises stress in the insulation for the cold load case.

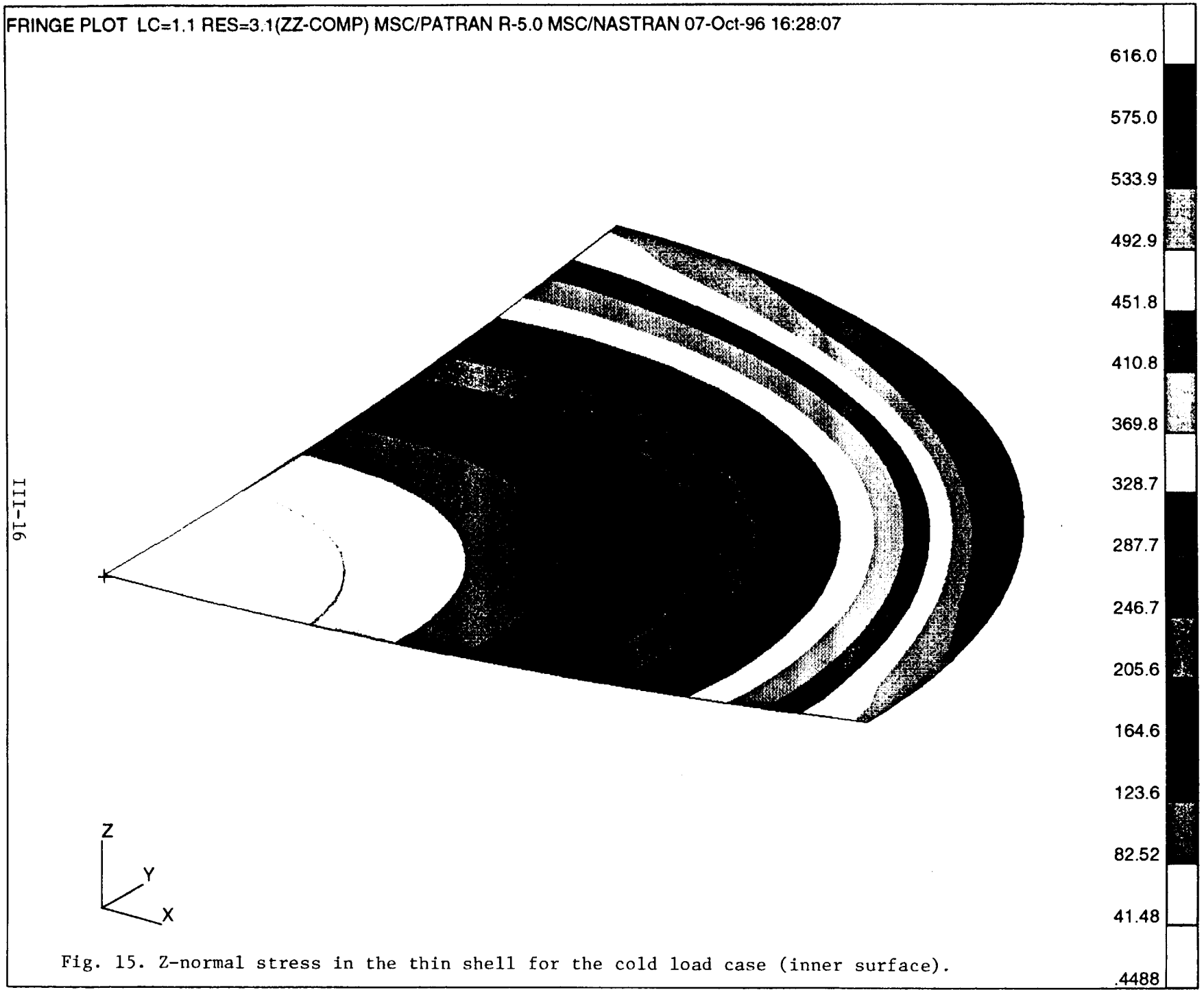

Fig. 15. Z-normal stress in the thin shell for the cold load case (inner surface).

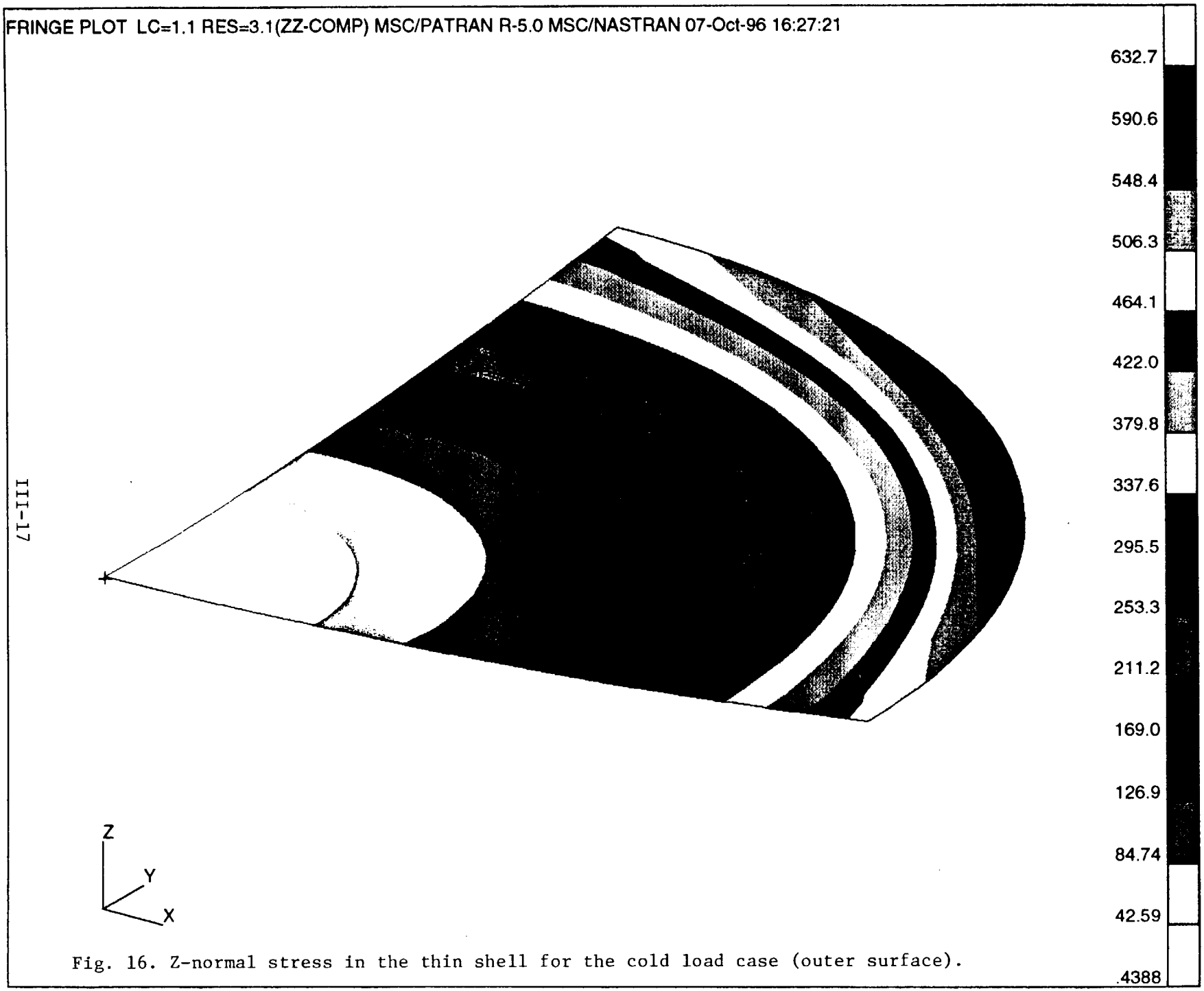

Fig. 16. Z-normal stress in the thin shell for the cold load case (outer surface).

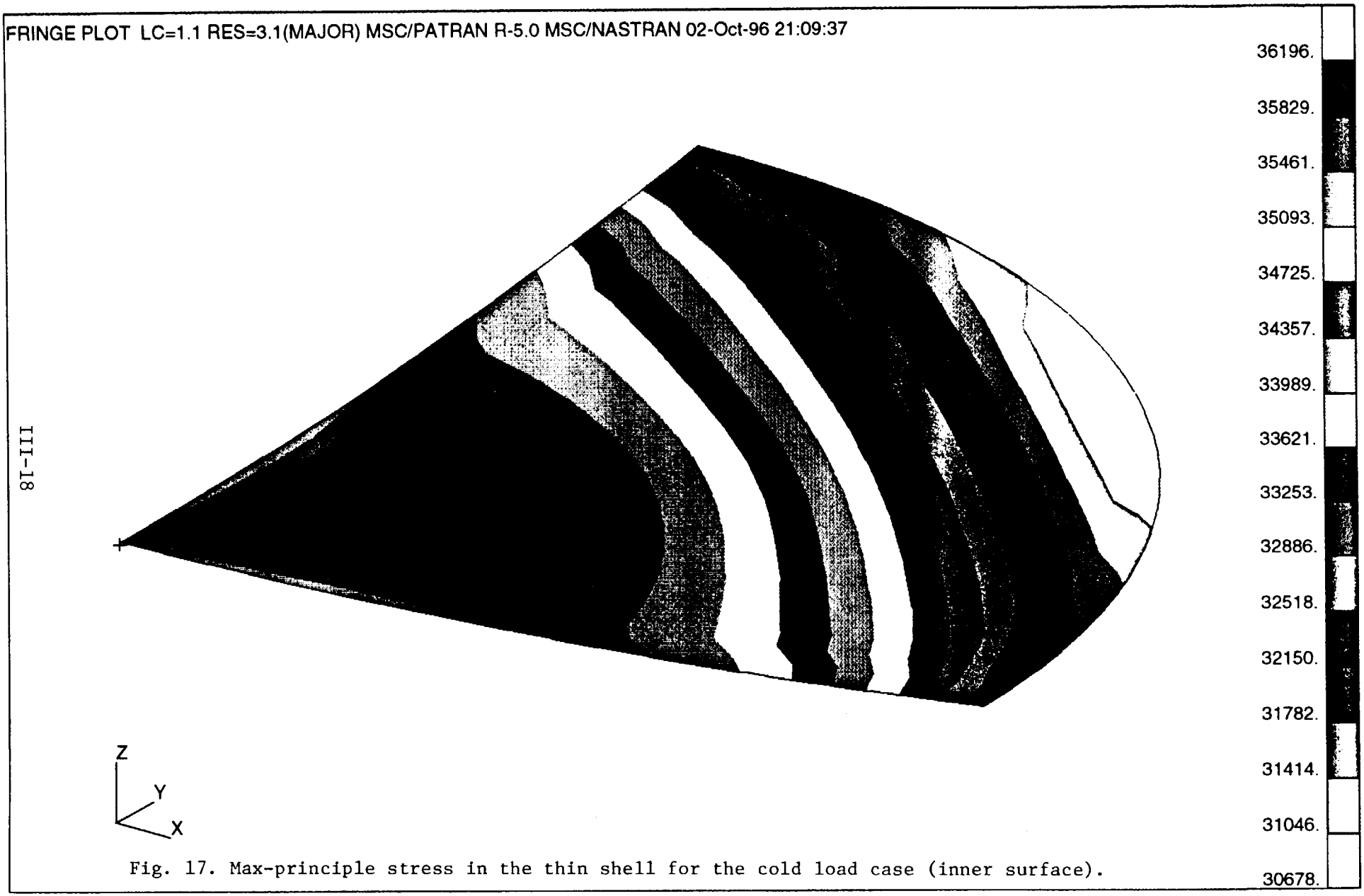

Fig. 17. Max-principle stress in the thin shell for the cold load case (inner surface).

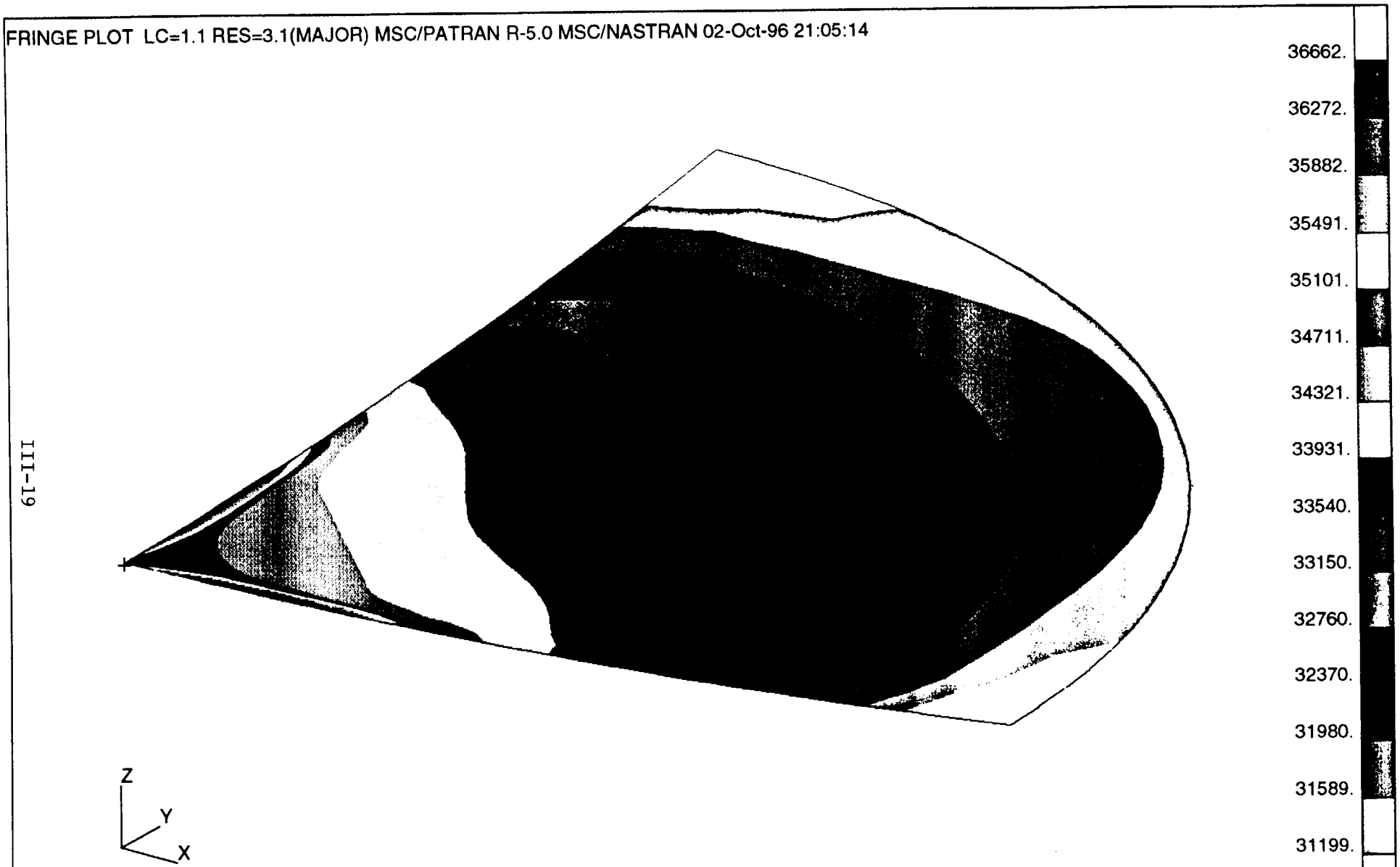

Fig. 18. Max-principle stress in the thin shell for the cold load case (outer surface).

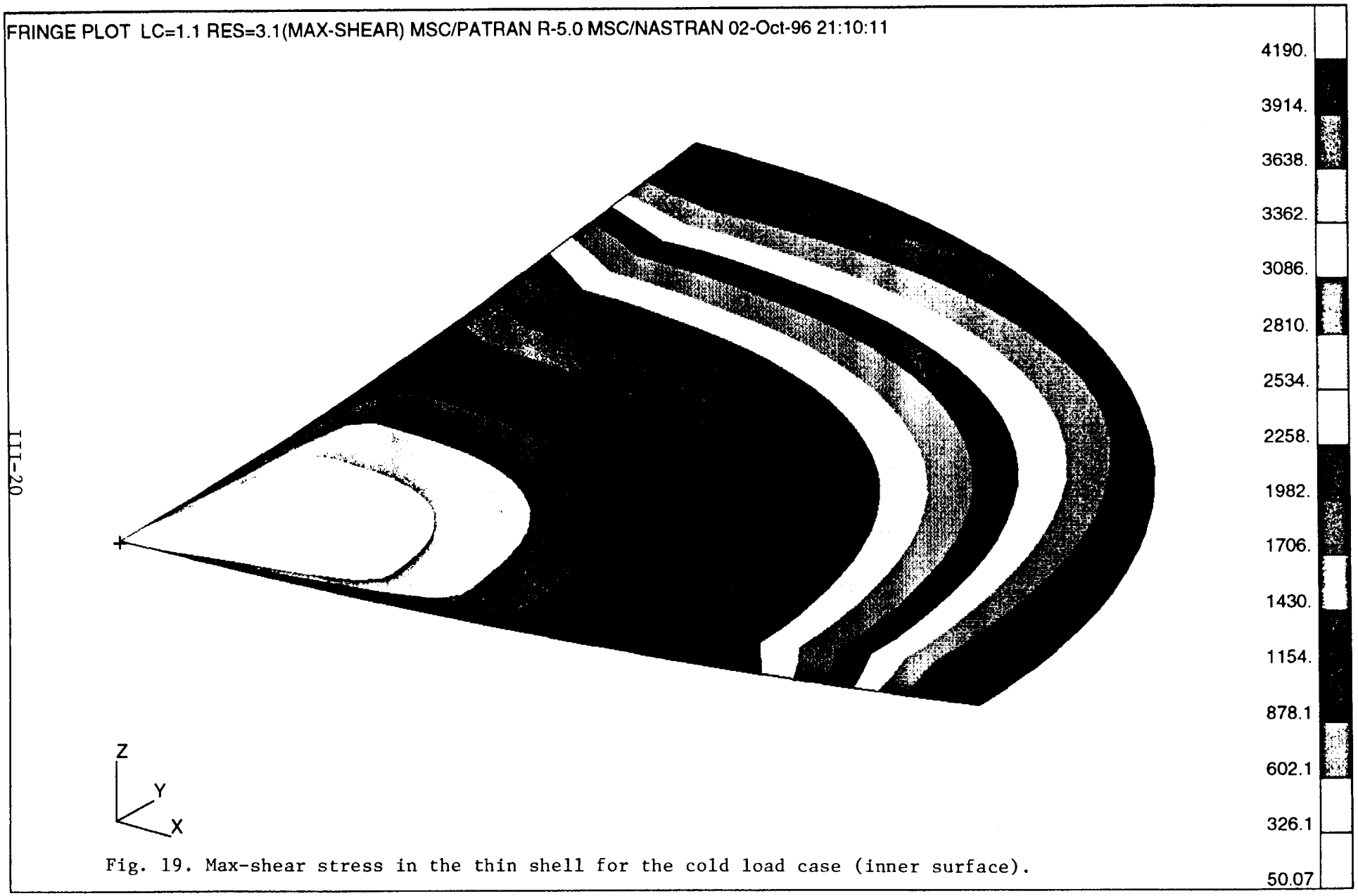

Fig. 19. Max-shear stress in the thin shell for the cold load case (inner surface).

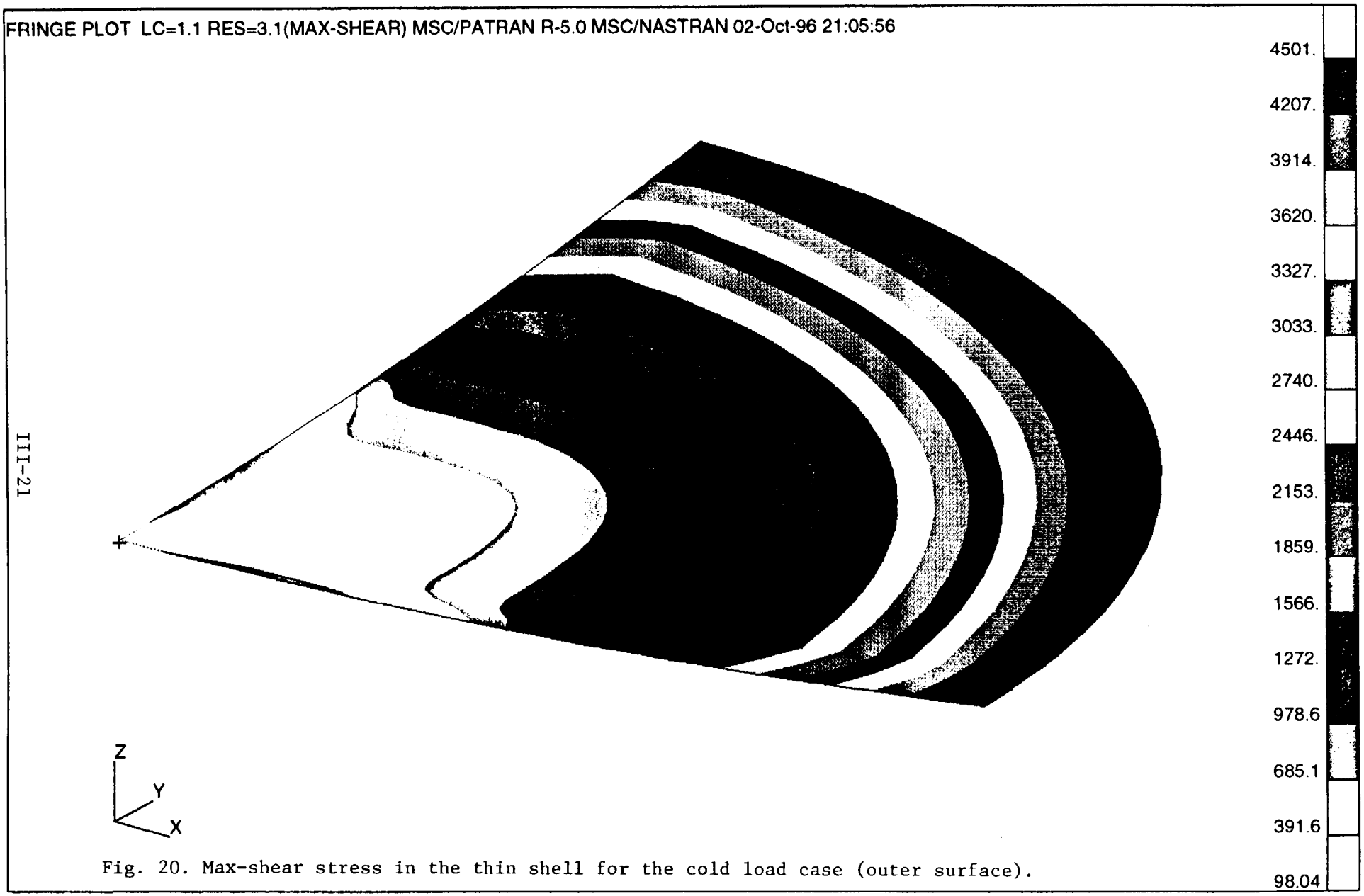

Fig. 20. Max-shear stress in the thin shell for the cold load case (outer surface).

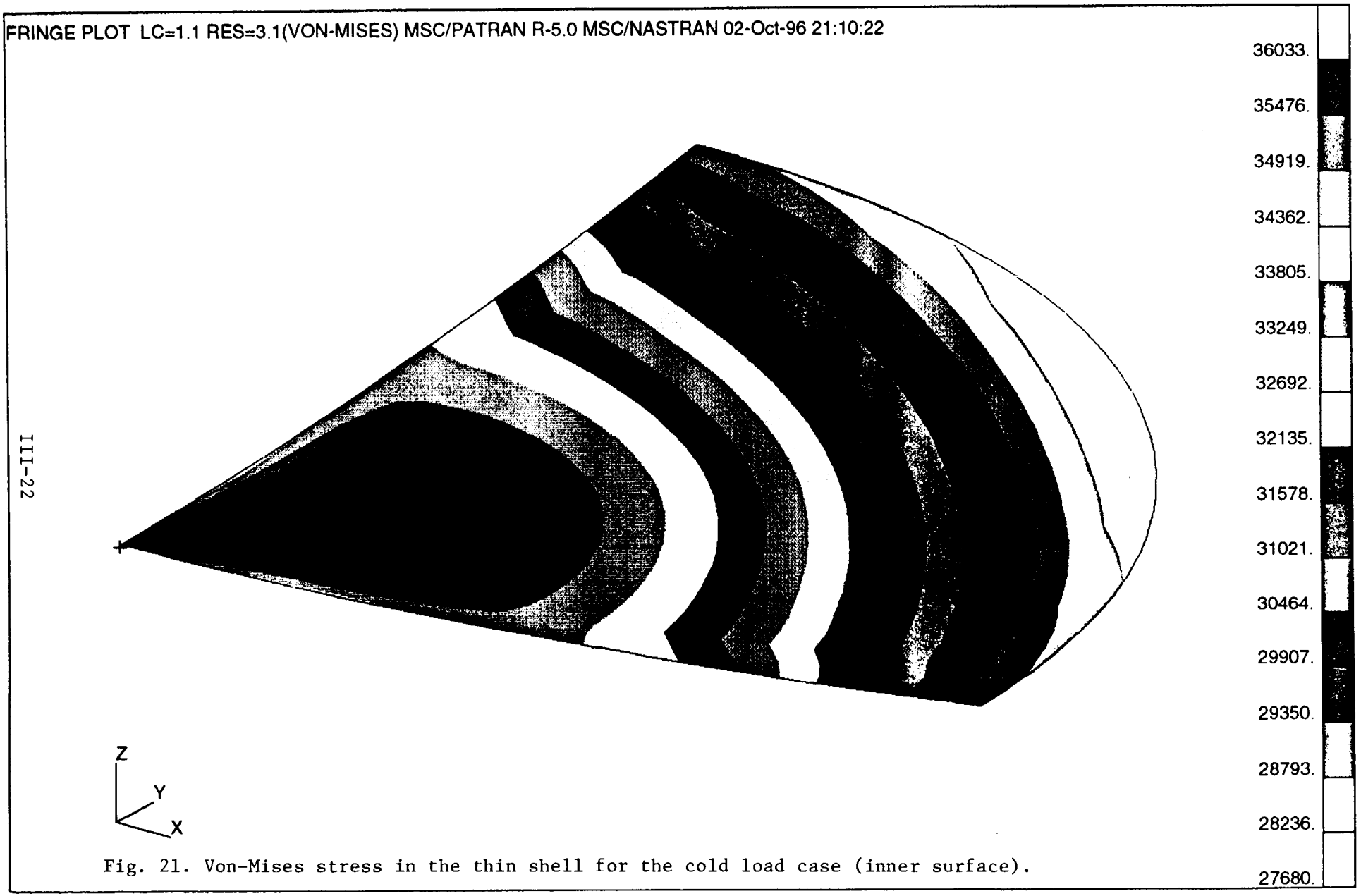

Fig. 21. Von-Mises stress in the thin shell for the cold load case (inner surface).

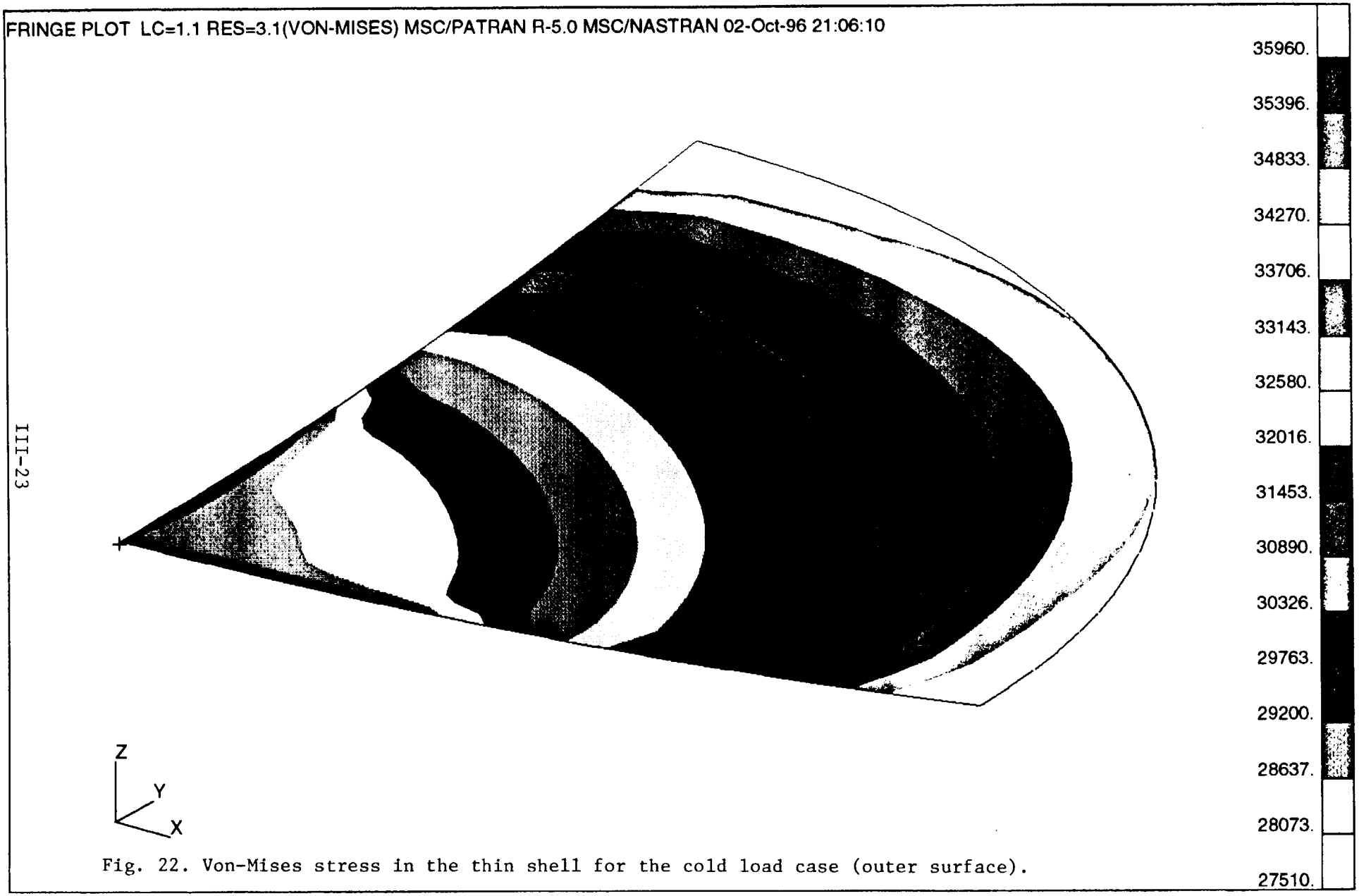

Fig. 22. Von-Mises stress in the thin shell for the cold load case (outer surface).

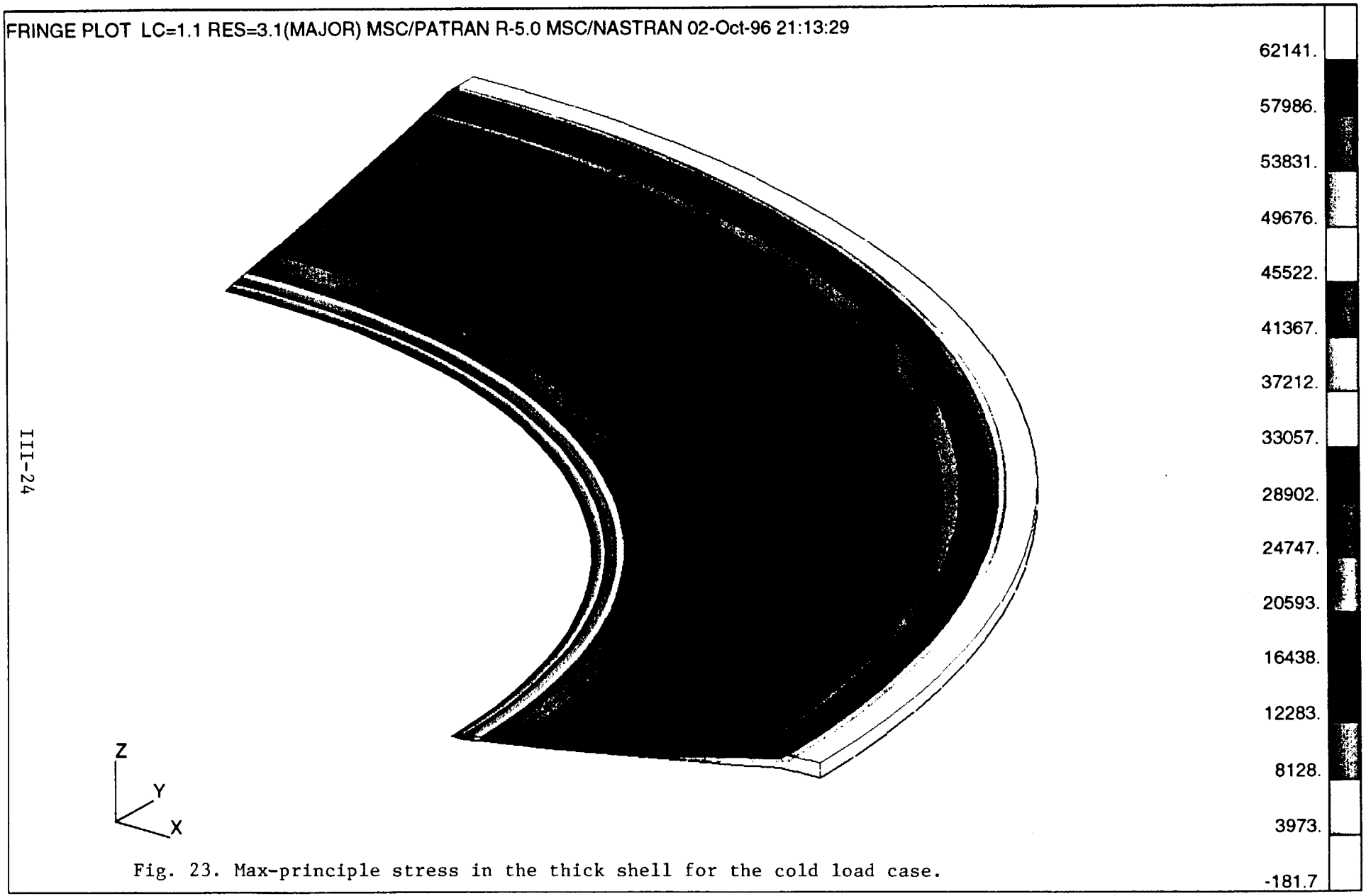

Fig. 23. Max-principle stress in the thick shell for the cold load case.

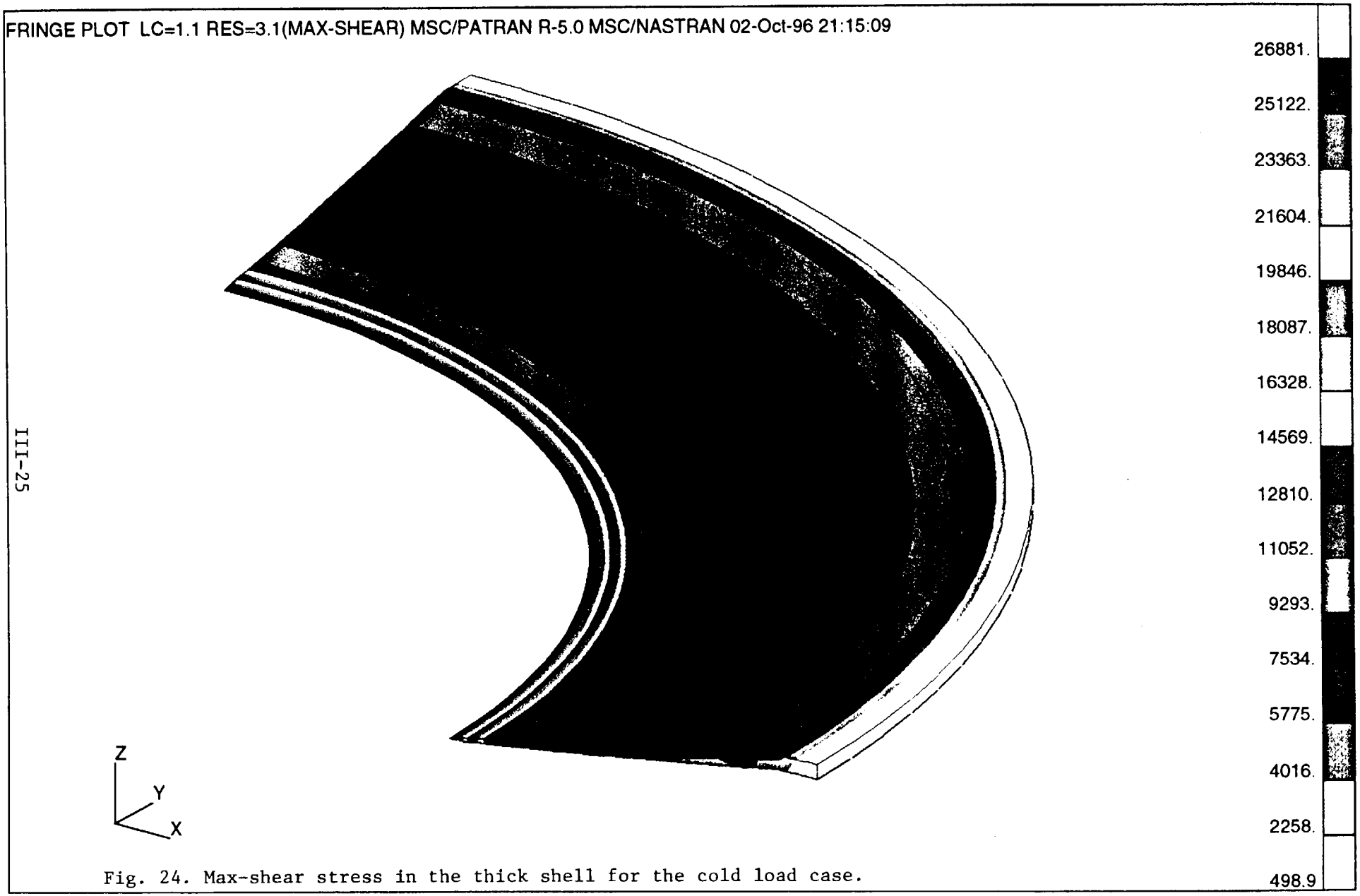

Fig. 24. Max-shear stress in the thick shell for the cold load case.

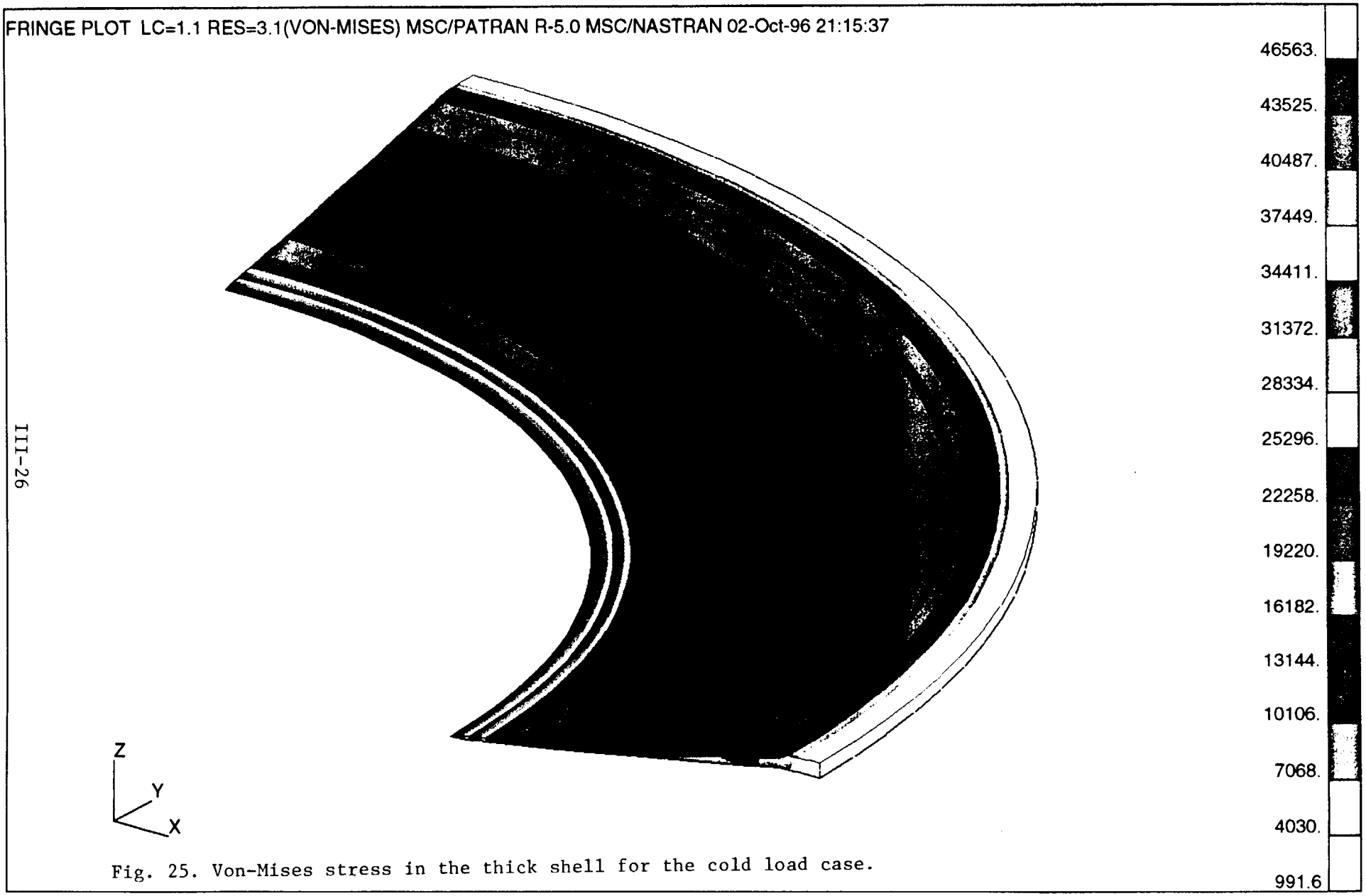

Fig. 25. Von-Mises stress in the thick shell for the cold load case.

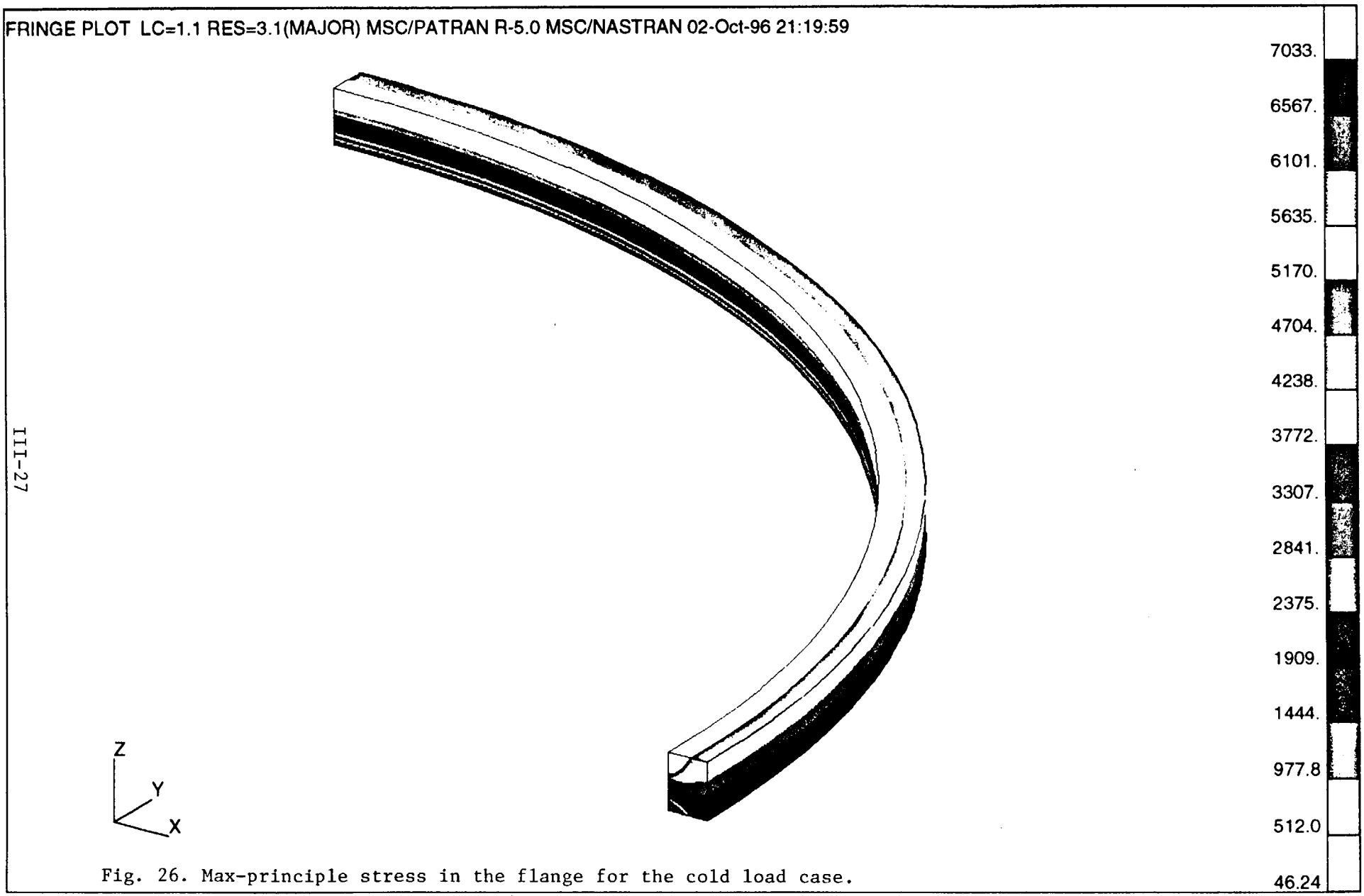

Fig. 26. Max-principle stress in the flange for the cold load case.

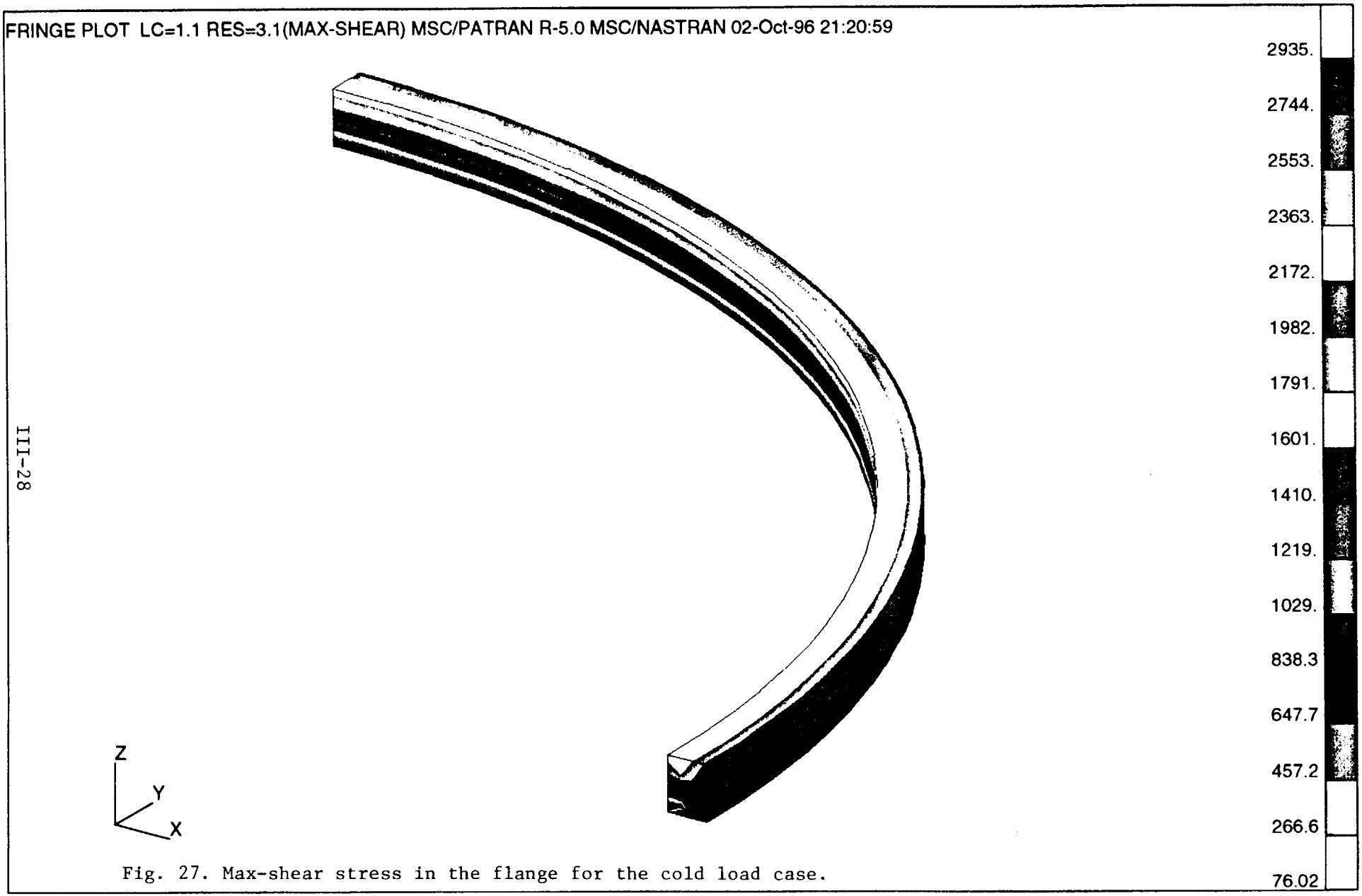

Fig. 27. Max-shear stress in the flange for the cold load case.

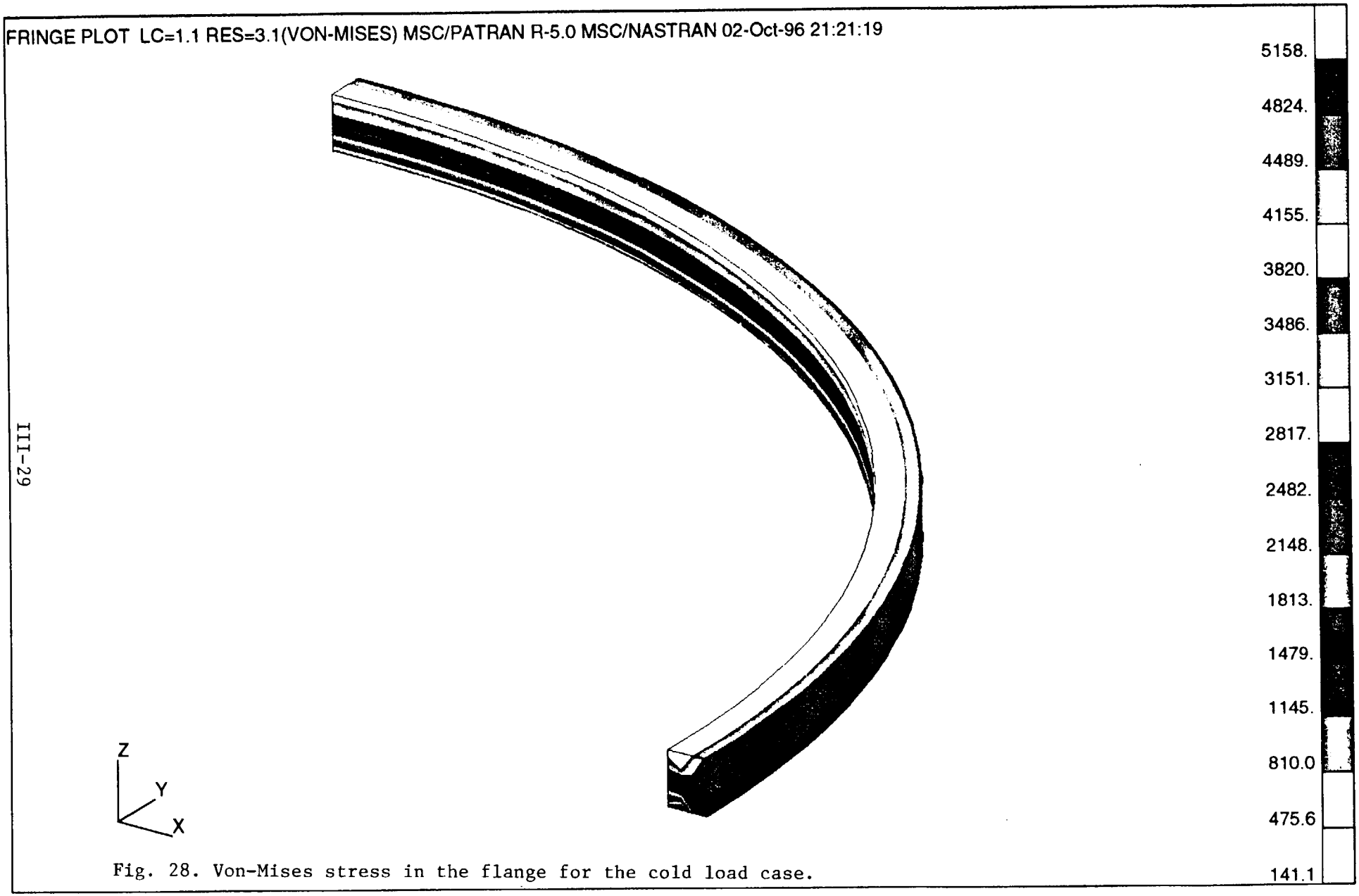

Fig. 28. Von-Mises stress in the flange for the cold load case.

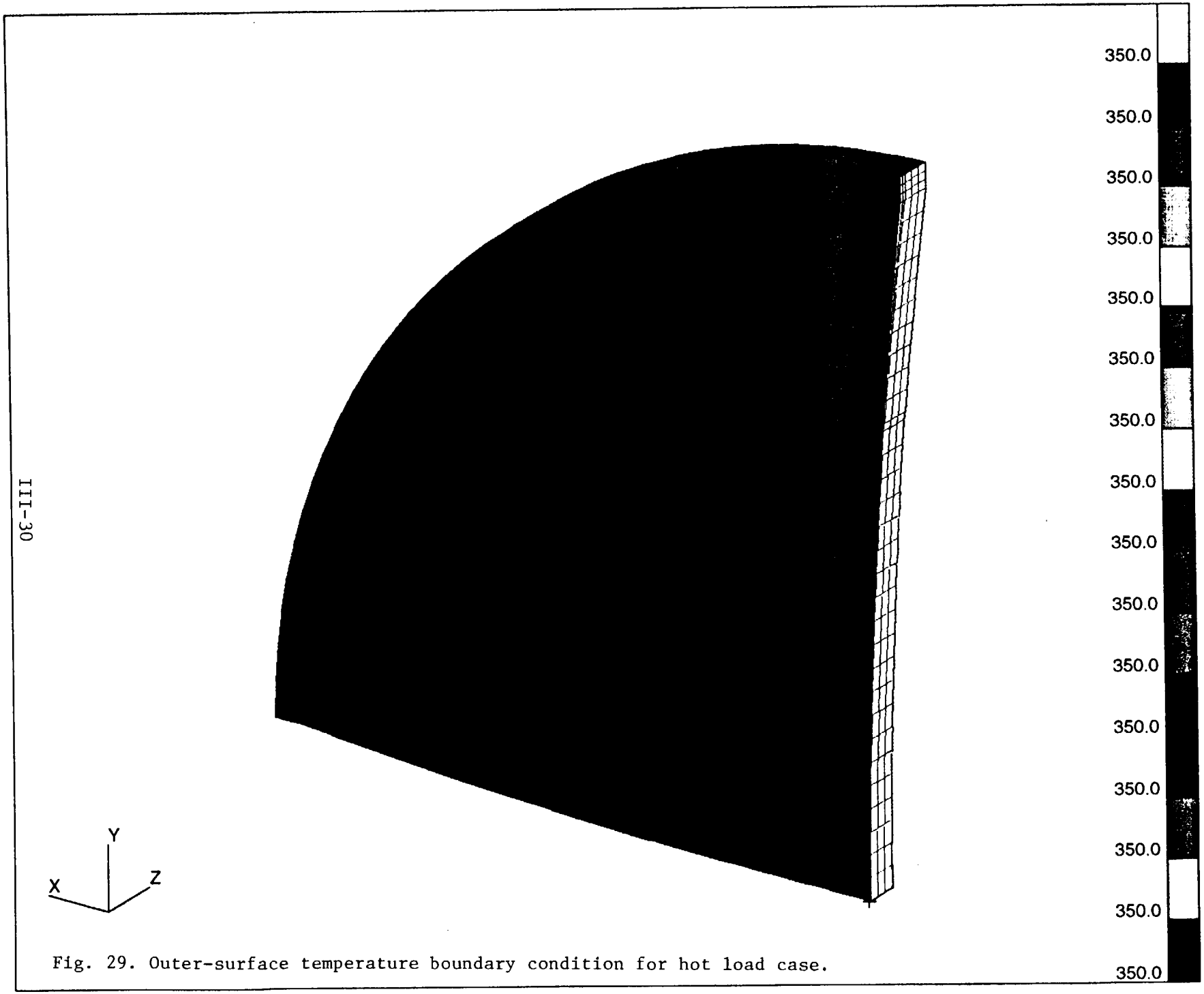

Fig. 29. Outer-surface temperature boundary condition for hot load case.

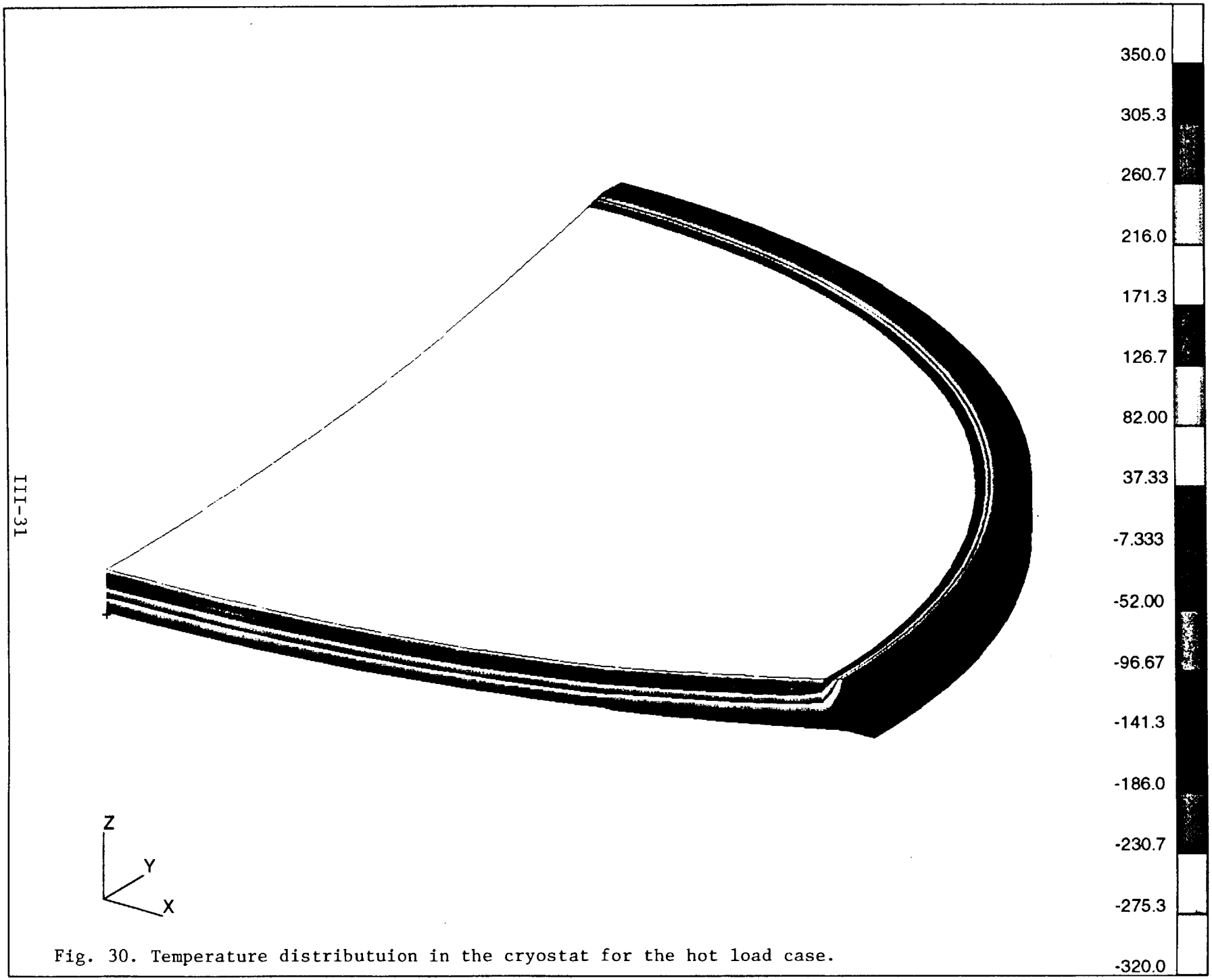

Fig. 30. Temperature distributuion in the cryostat for the hot load case.

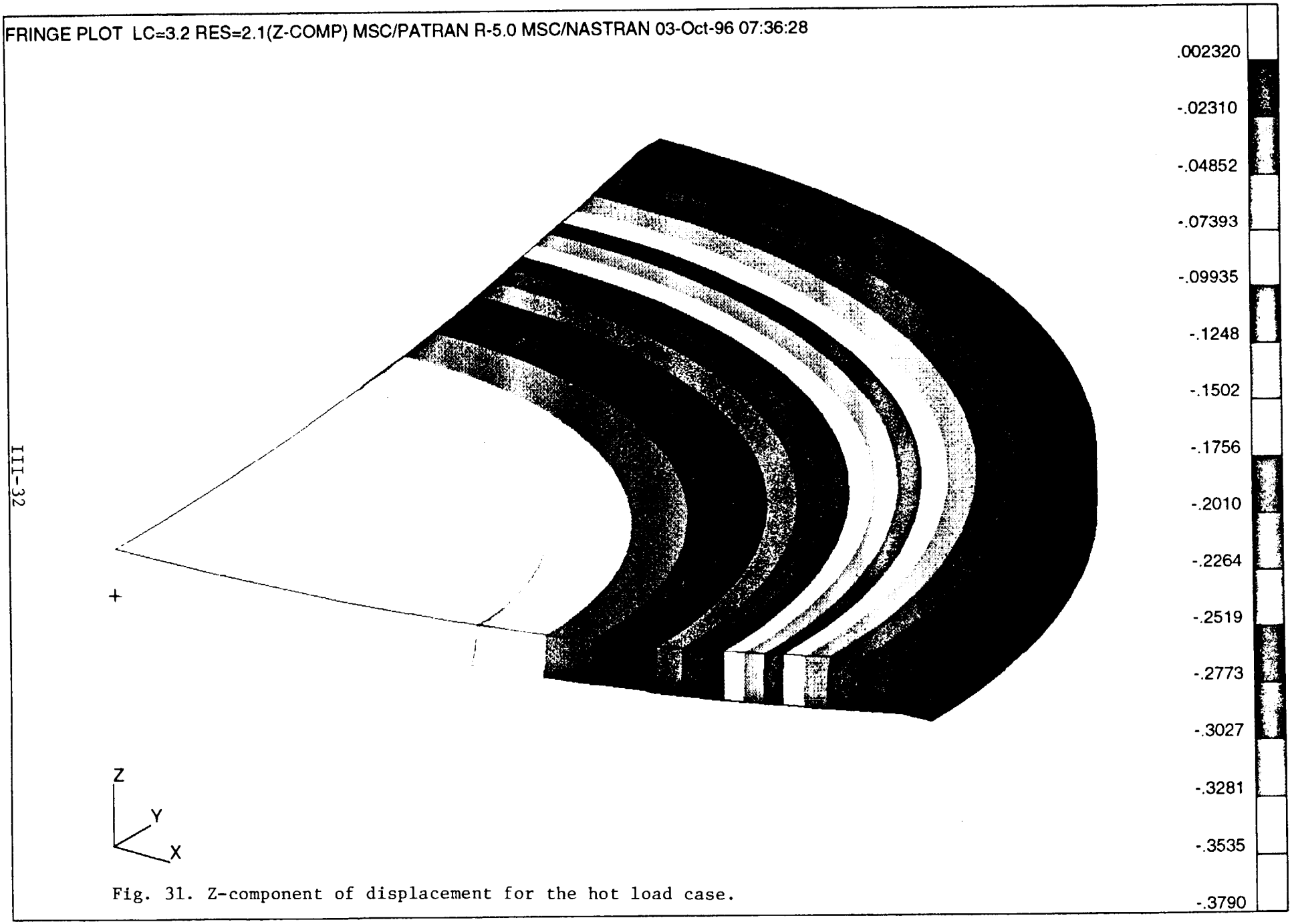

Fig. 31. Z-component of displacement for the hot load case.

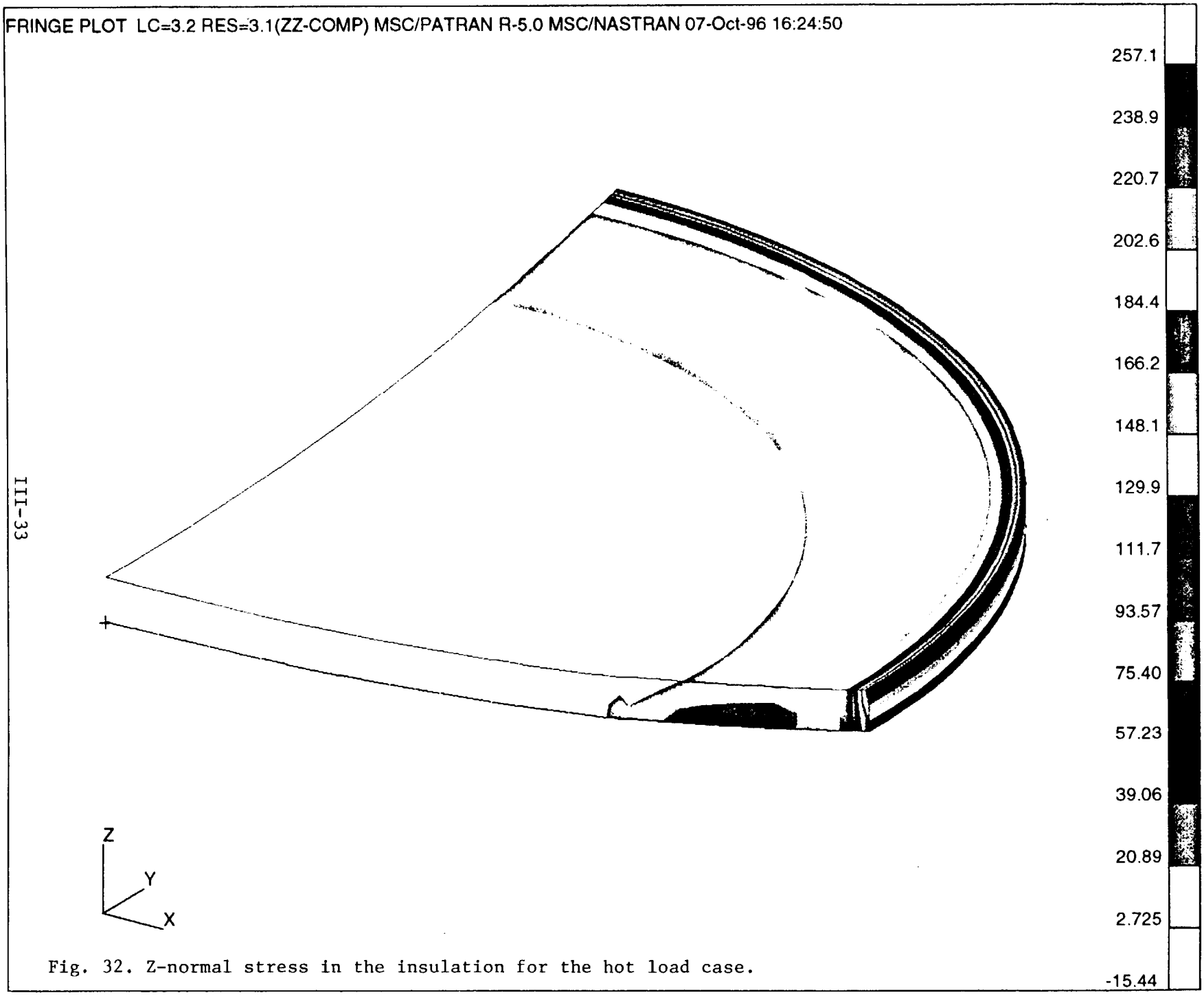

Fig. 32. Z-normal stress in the insulation for the hot load case.

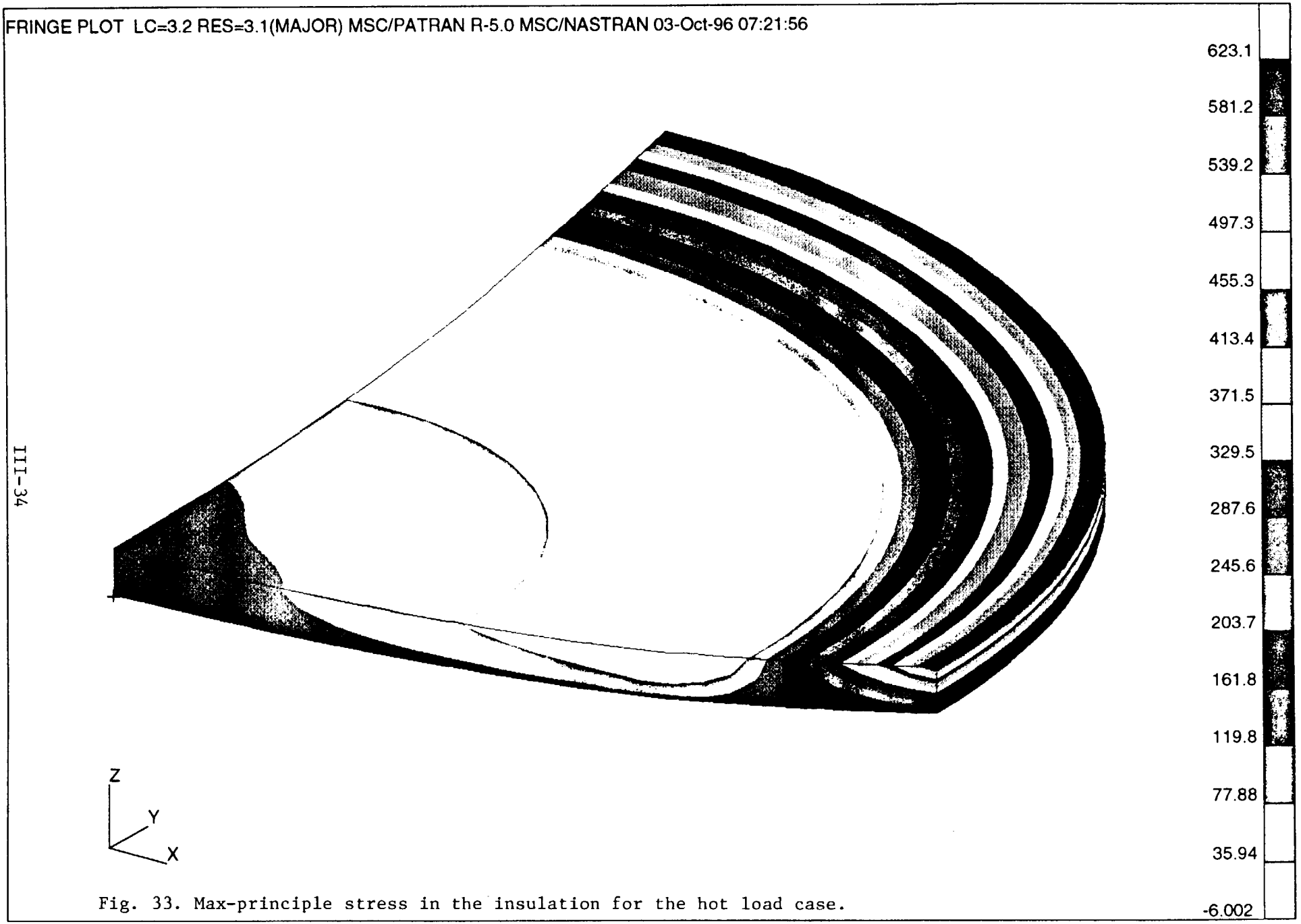

Fig. 33. Max-principle stress in the insulation for the hot load case.

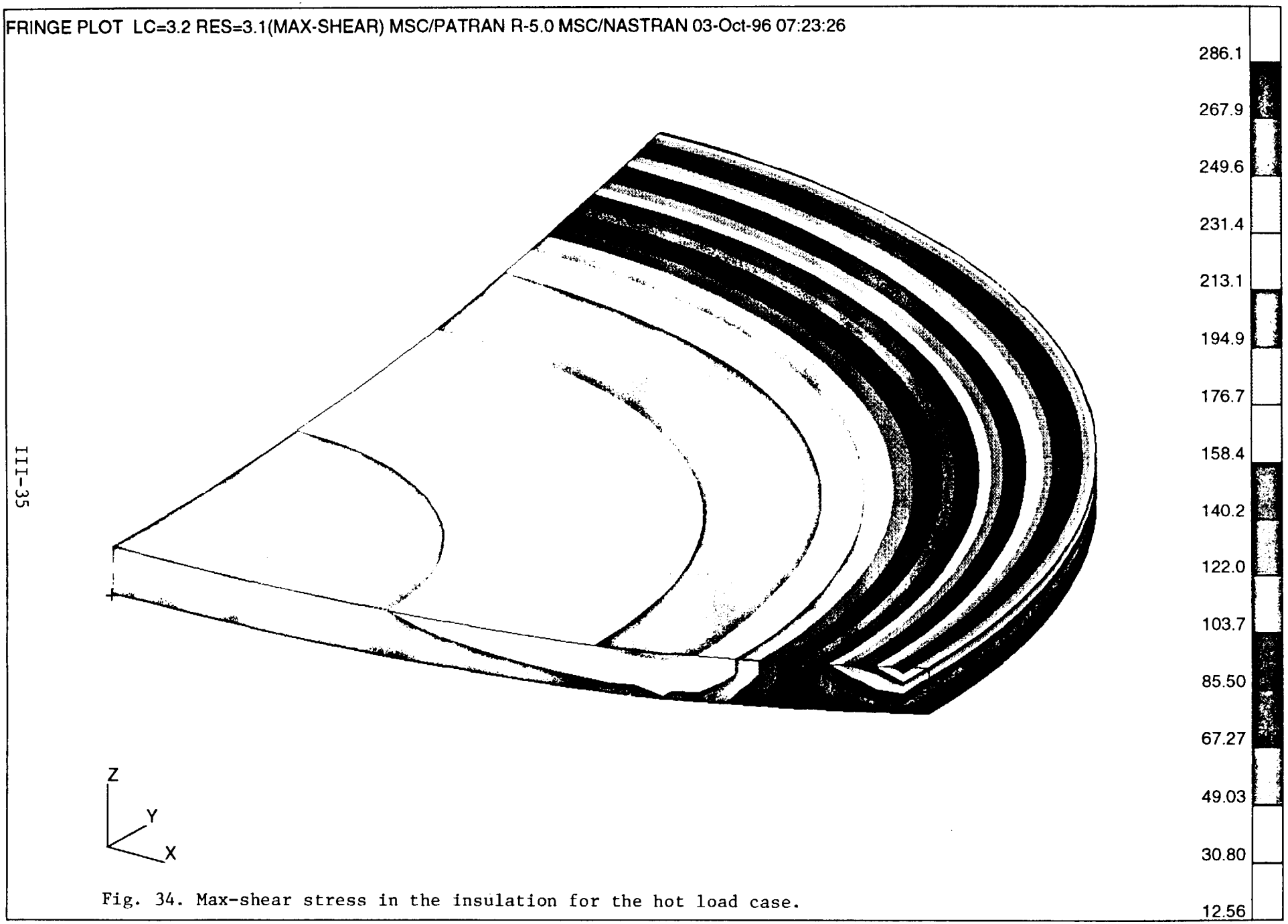

Fig. 34. Max-shear stress in the insulation for the hot load case.

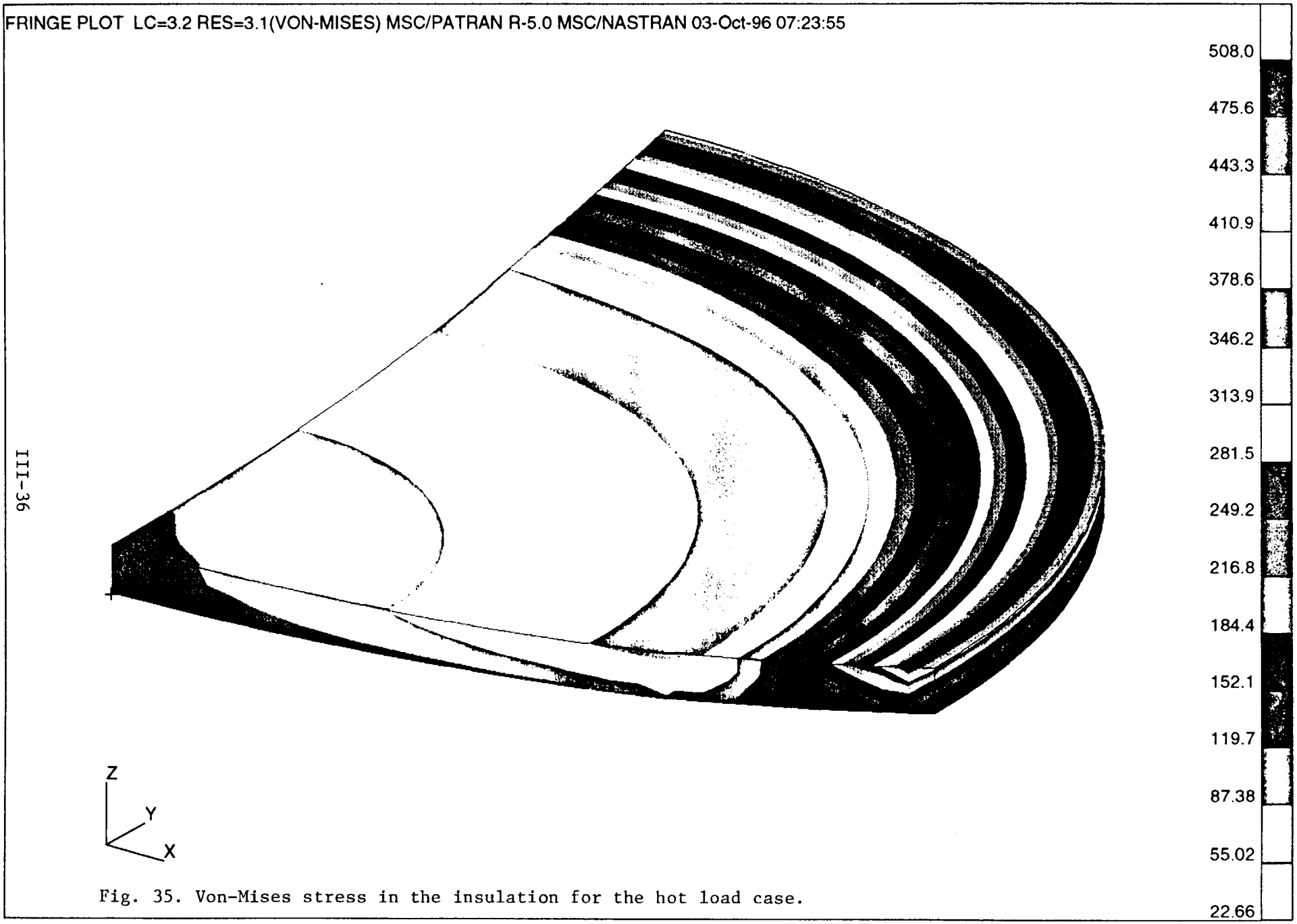

Fig. 35. Von-Mises stress in the insulation for the hot load case.

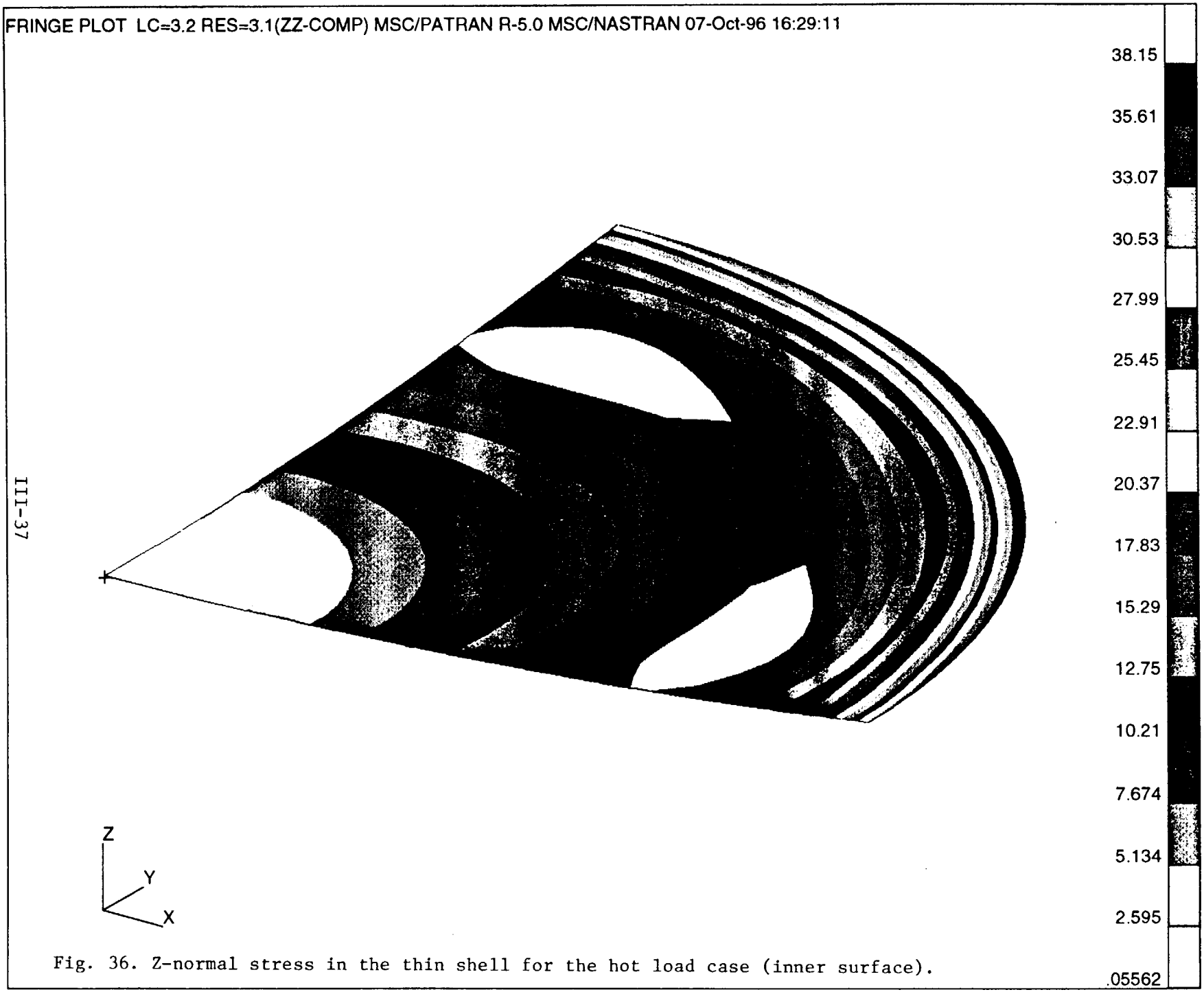

Fig. 36. Z-normal stress in the thin shell for the hot load case (inner surface).

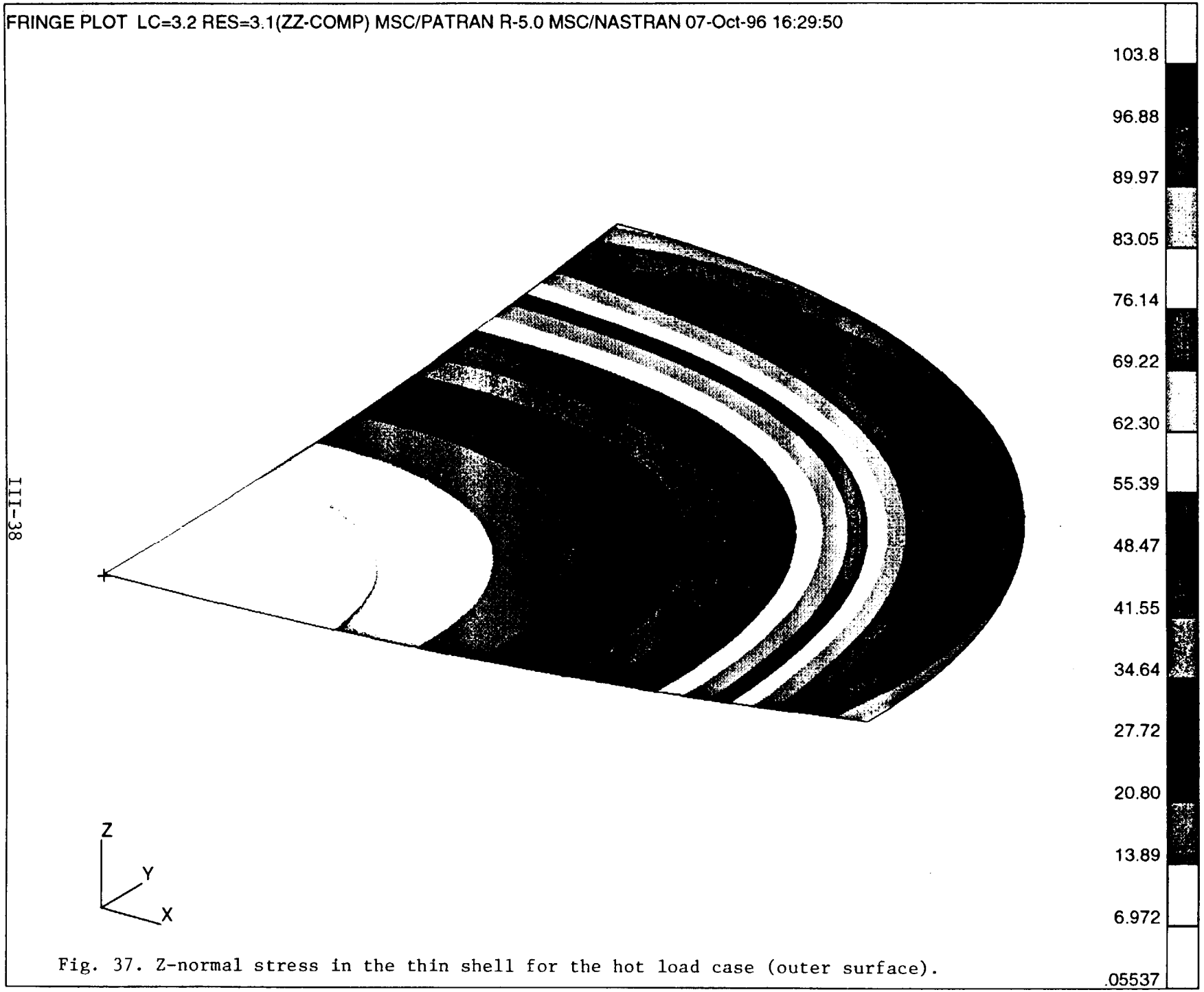

Fig. 37. Z-normal stress in the thin shell for the hot load case (outer surface).

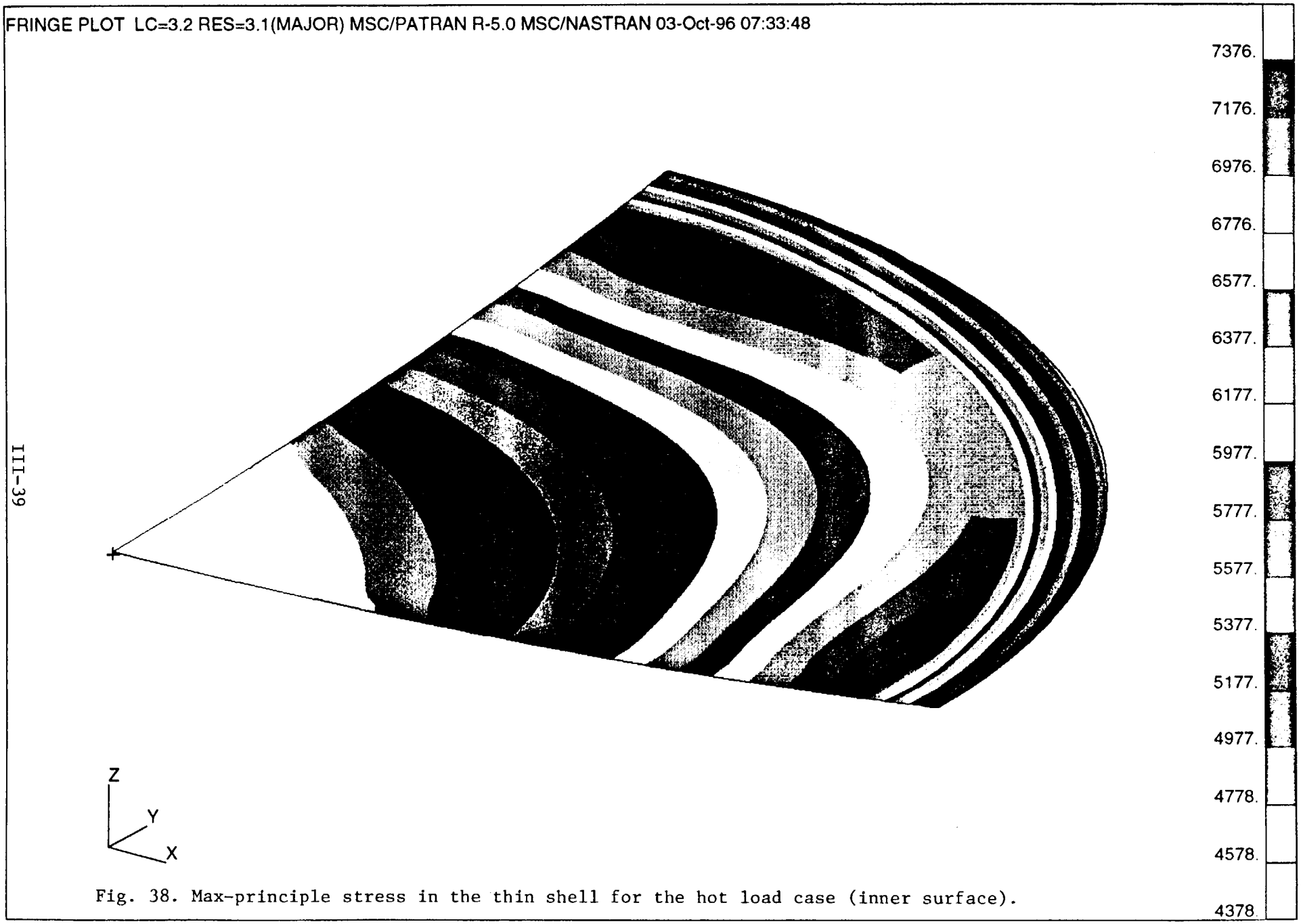

Fig. 38. Max-principle stress in the thin shell for the hot load case (inner surface).

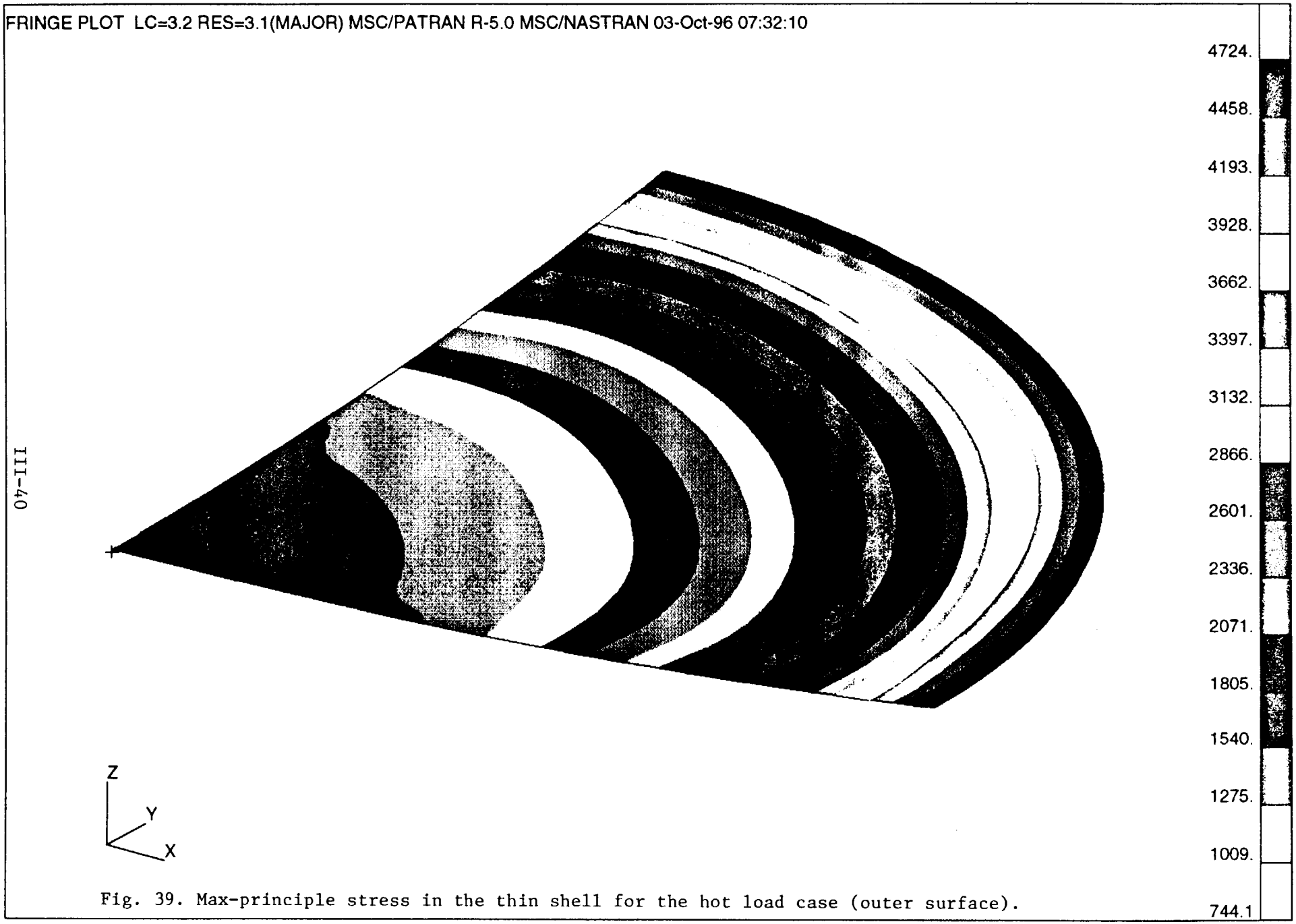

Fig. 39. Max-principle stress in the thin shell for the hot load case (outer surface).

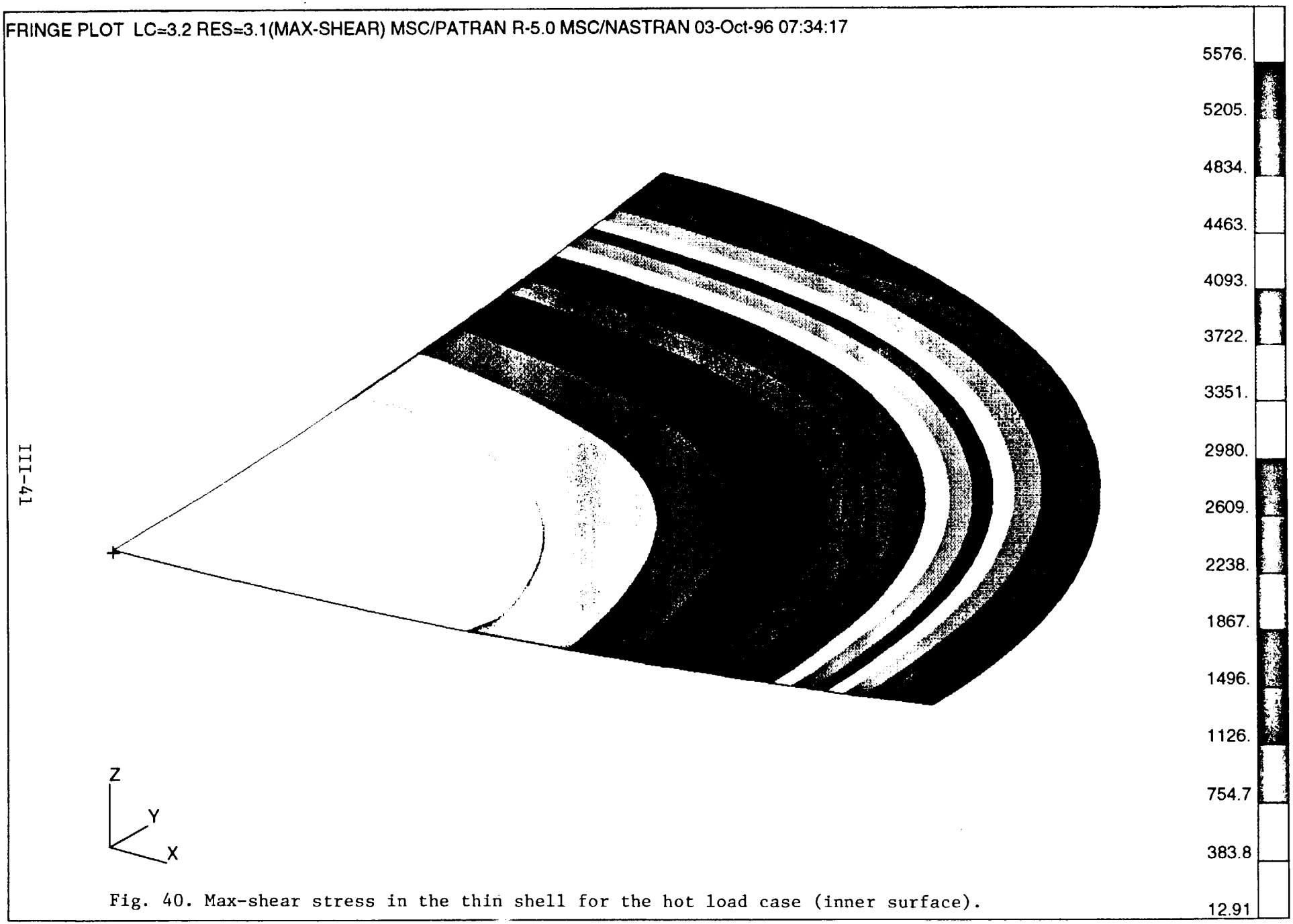

Fig. 40. Max-shear stress in the thin shell for the hot load case (inner surface).

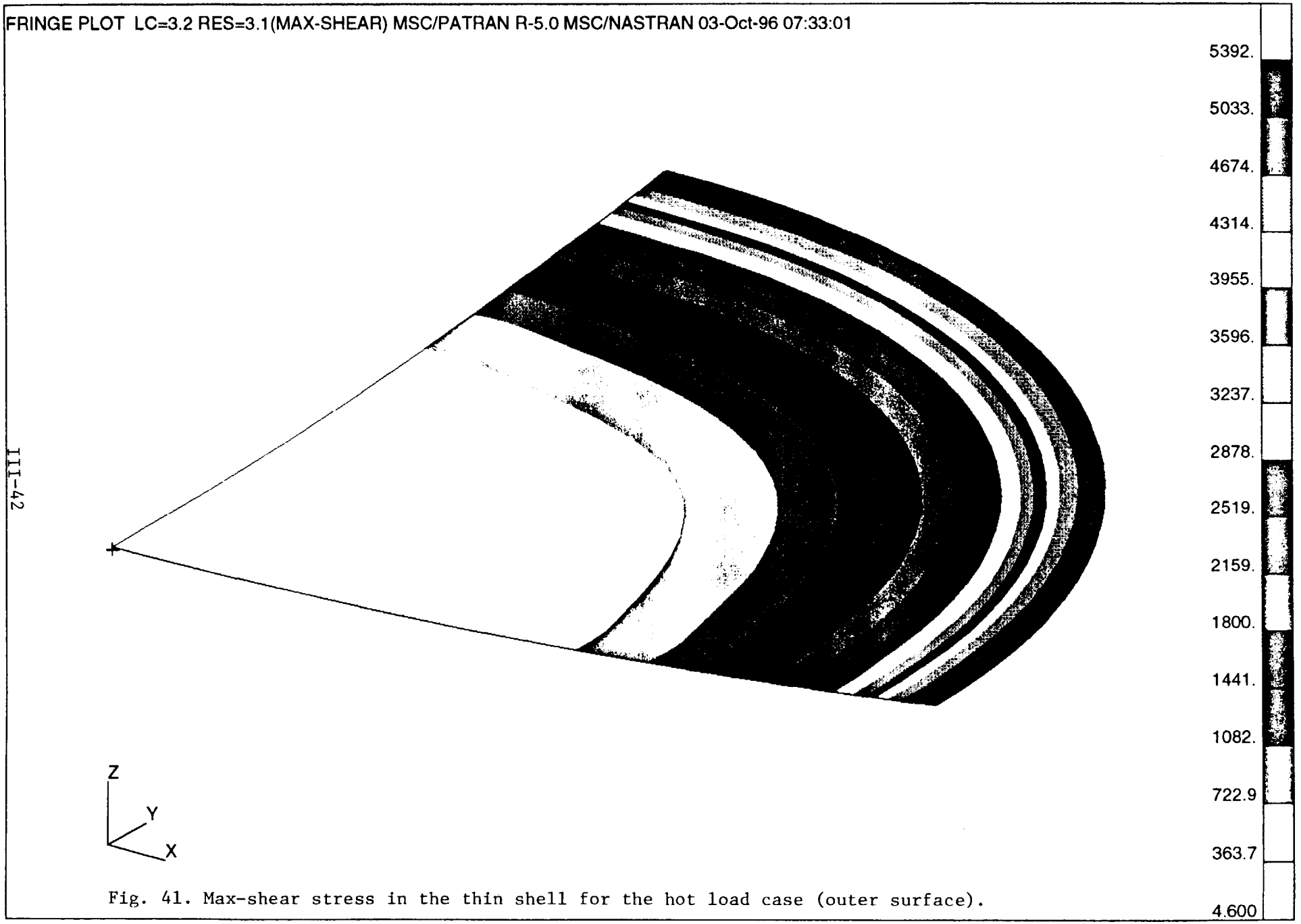

Fig. 41. Max-shear stress in the thin shell for the hot load case (outer surface).

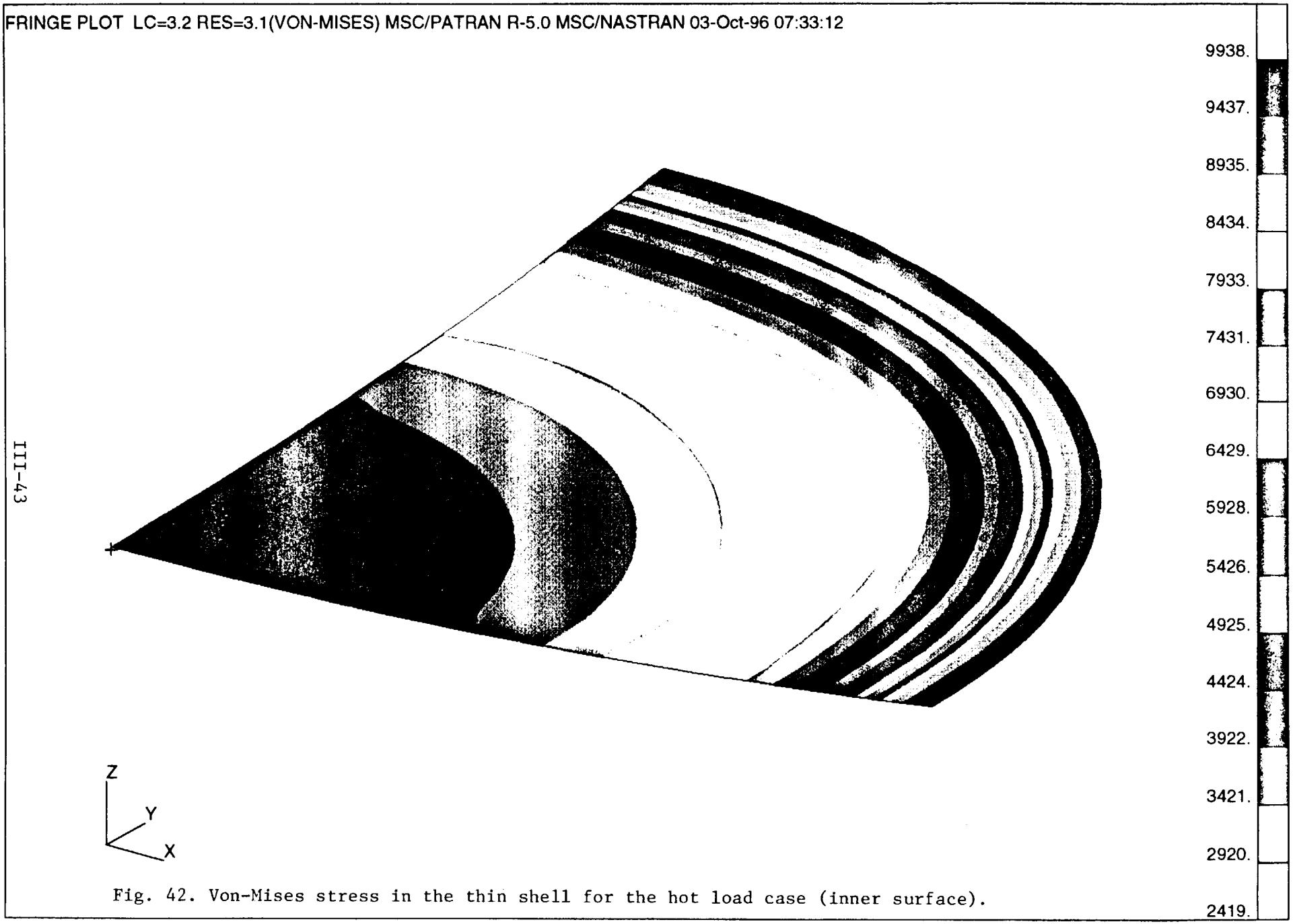

Fig. 42. Von-Mises stress in the thin shell for the hot load case (inner surface).

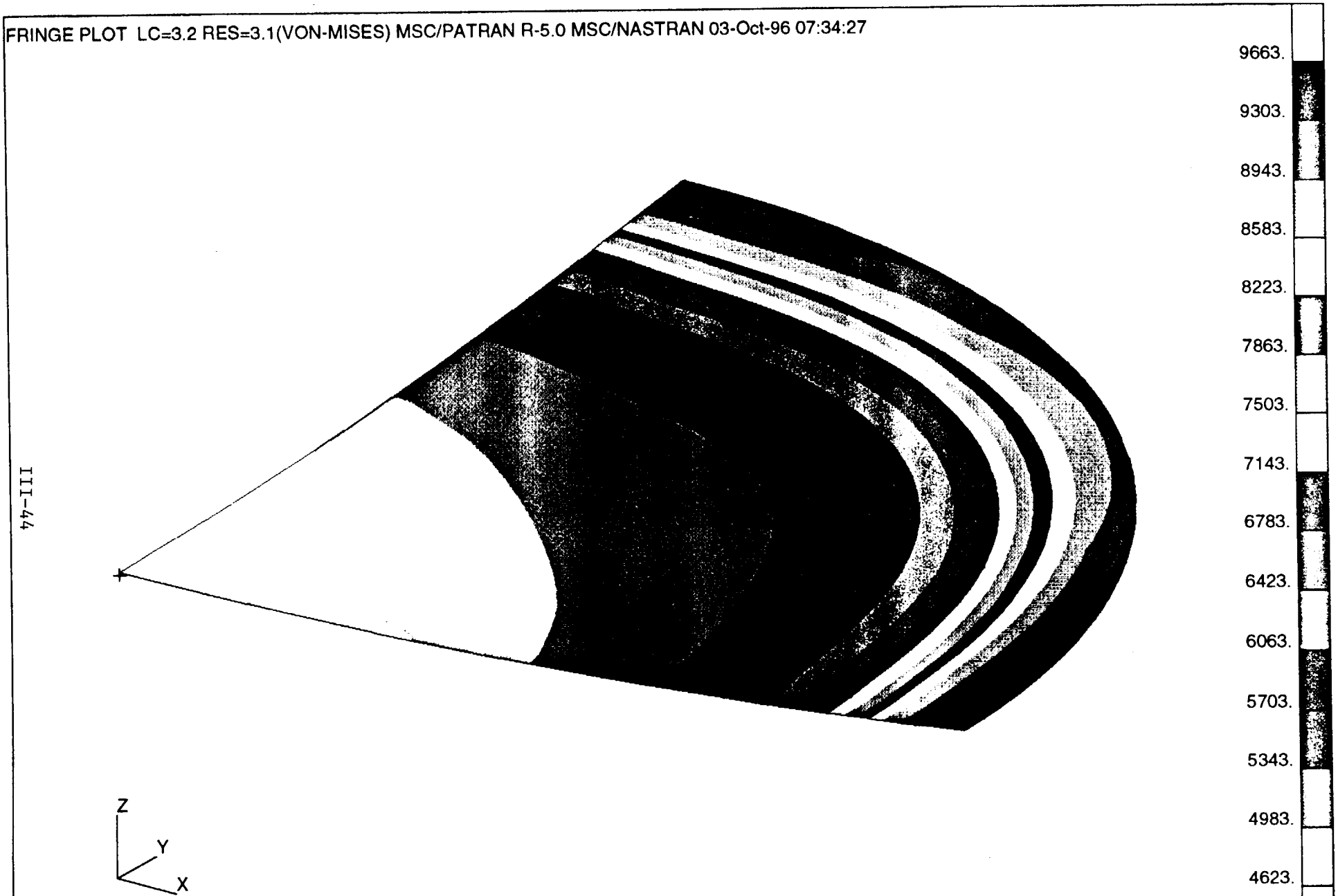

Fig. 43. Von-Mises stress in the thin shell for the hot load case (outer surface).

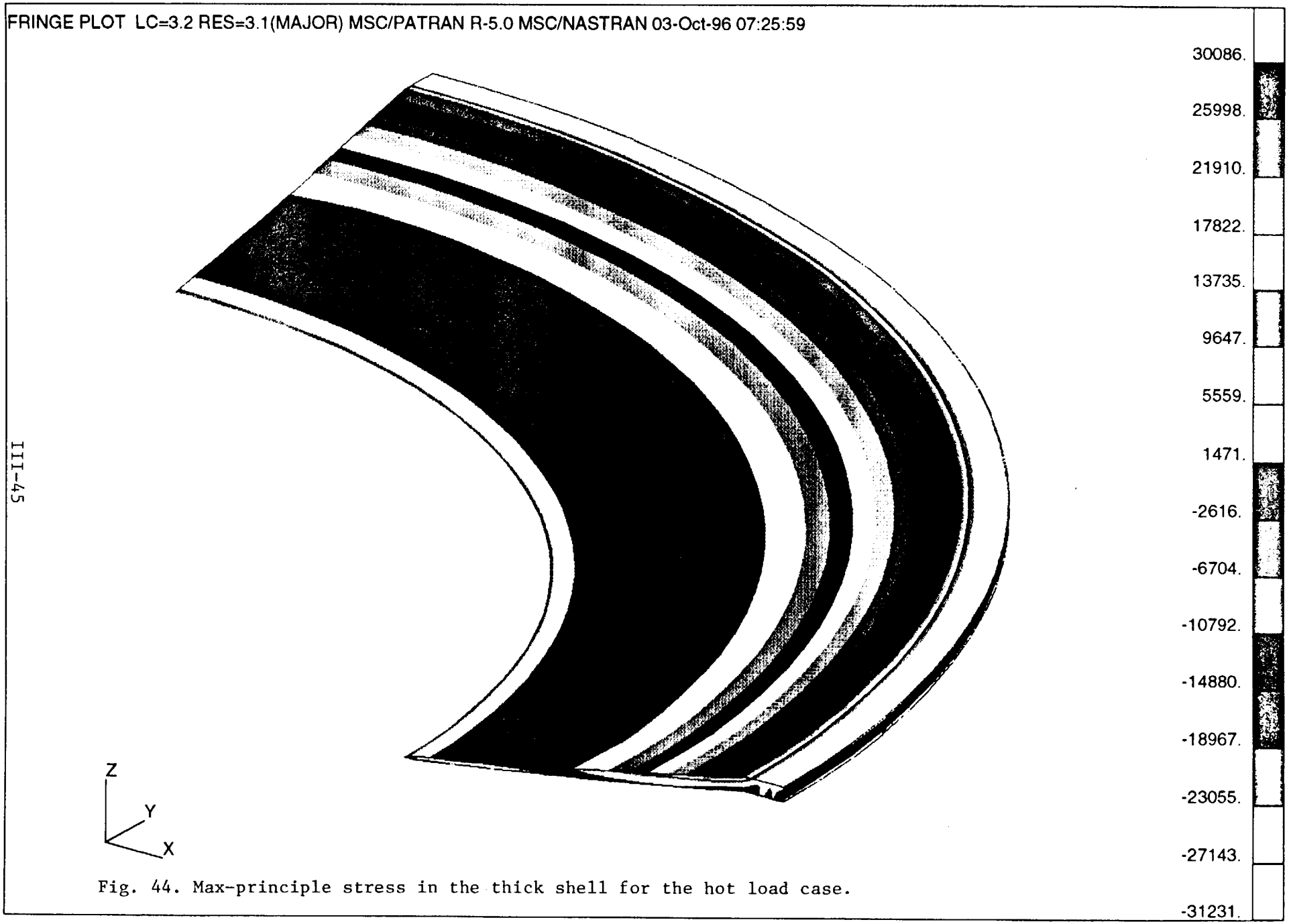

Fig. 44. Max-principle stress in the thick shell for the hot load case.

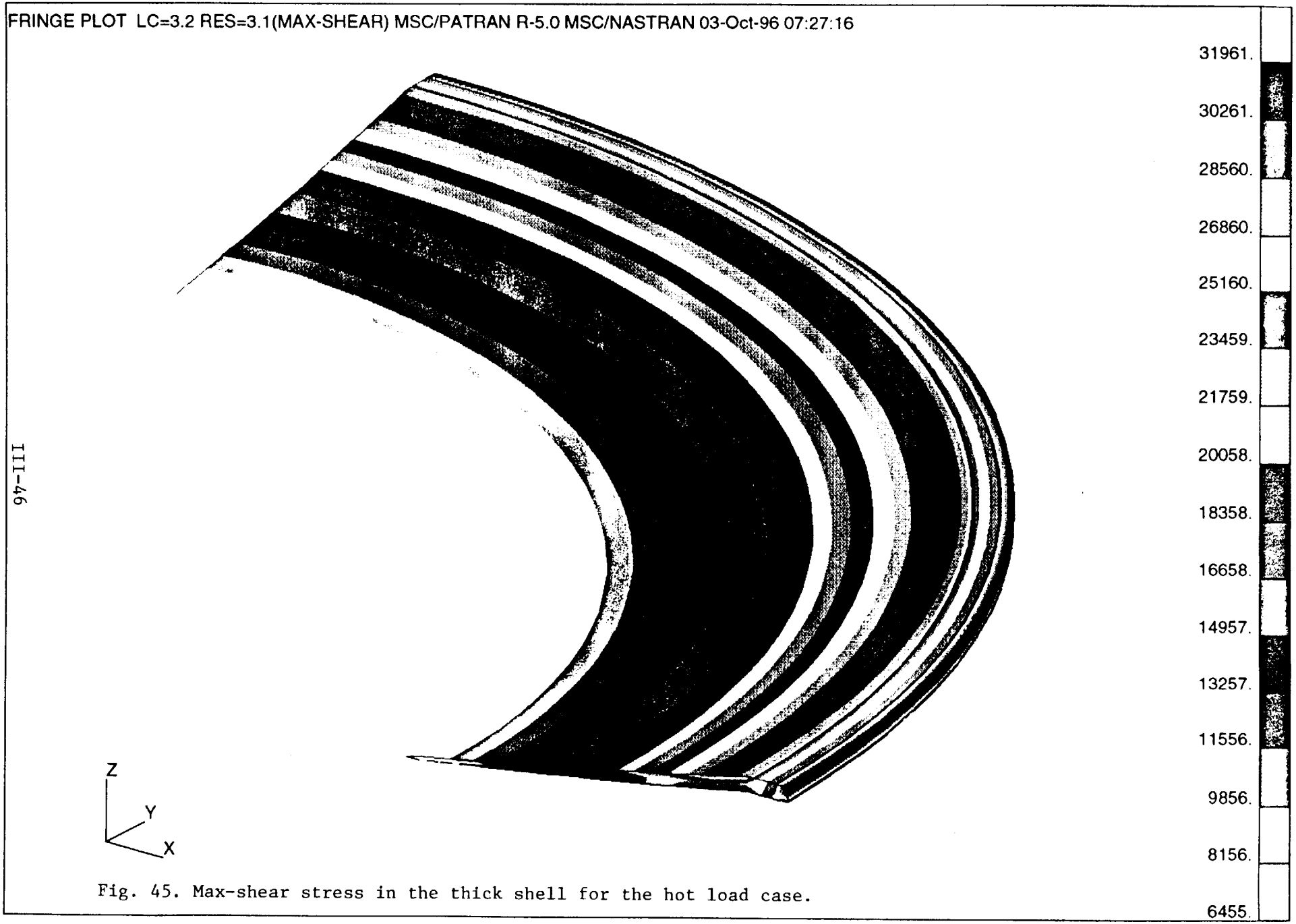

Fig. 45. Max-shear stress in the thick shell for the hot load case.

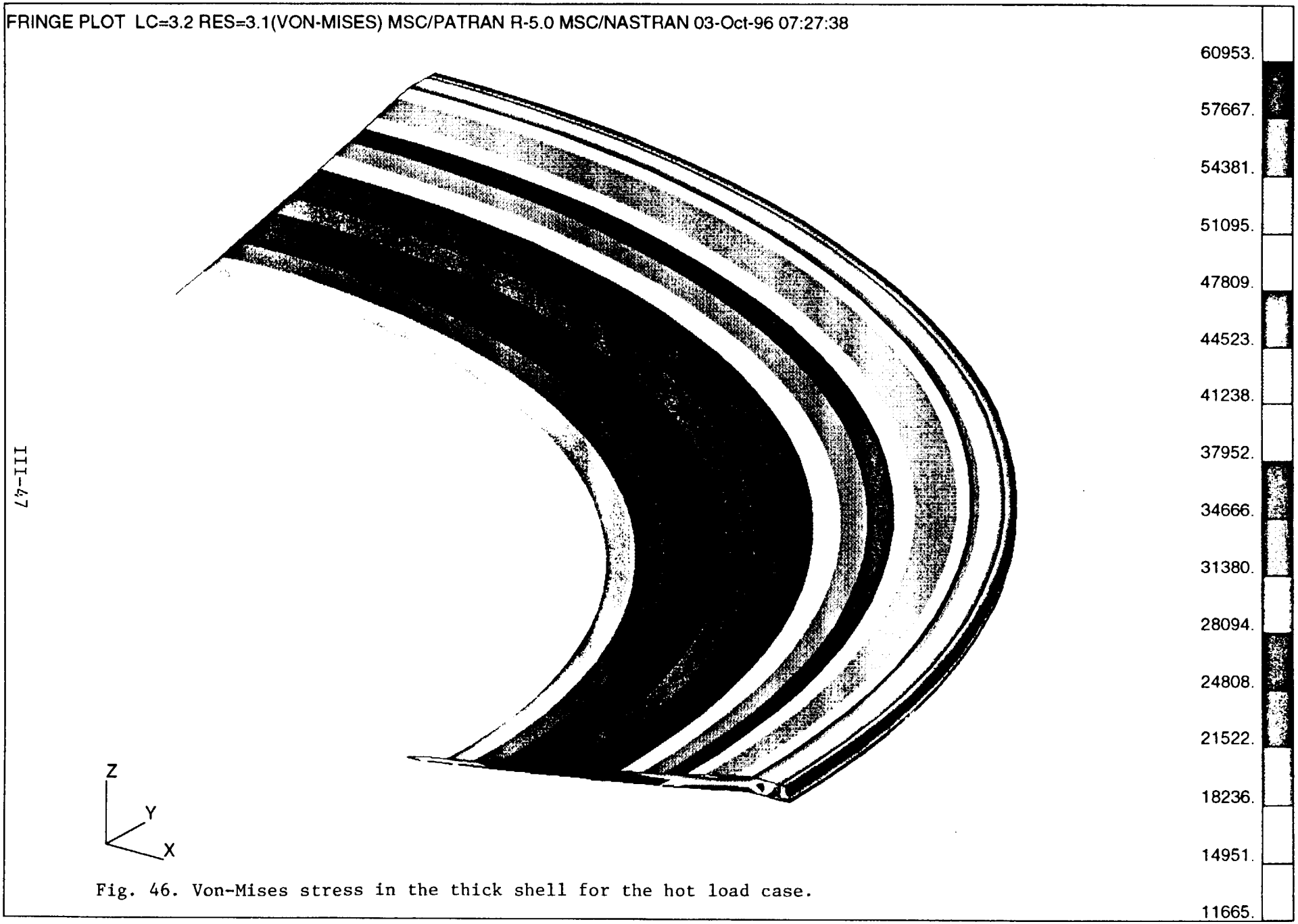

Fig. 46. Von-Mises stress in the thick shell for the hot load case.

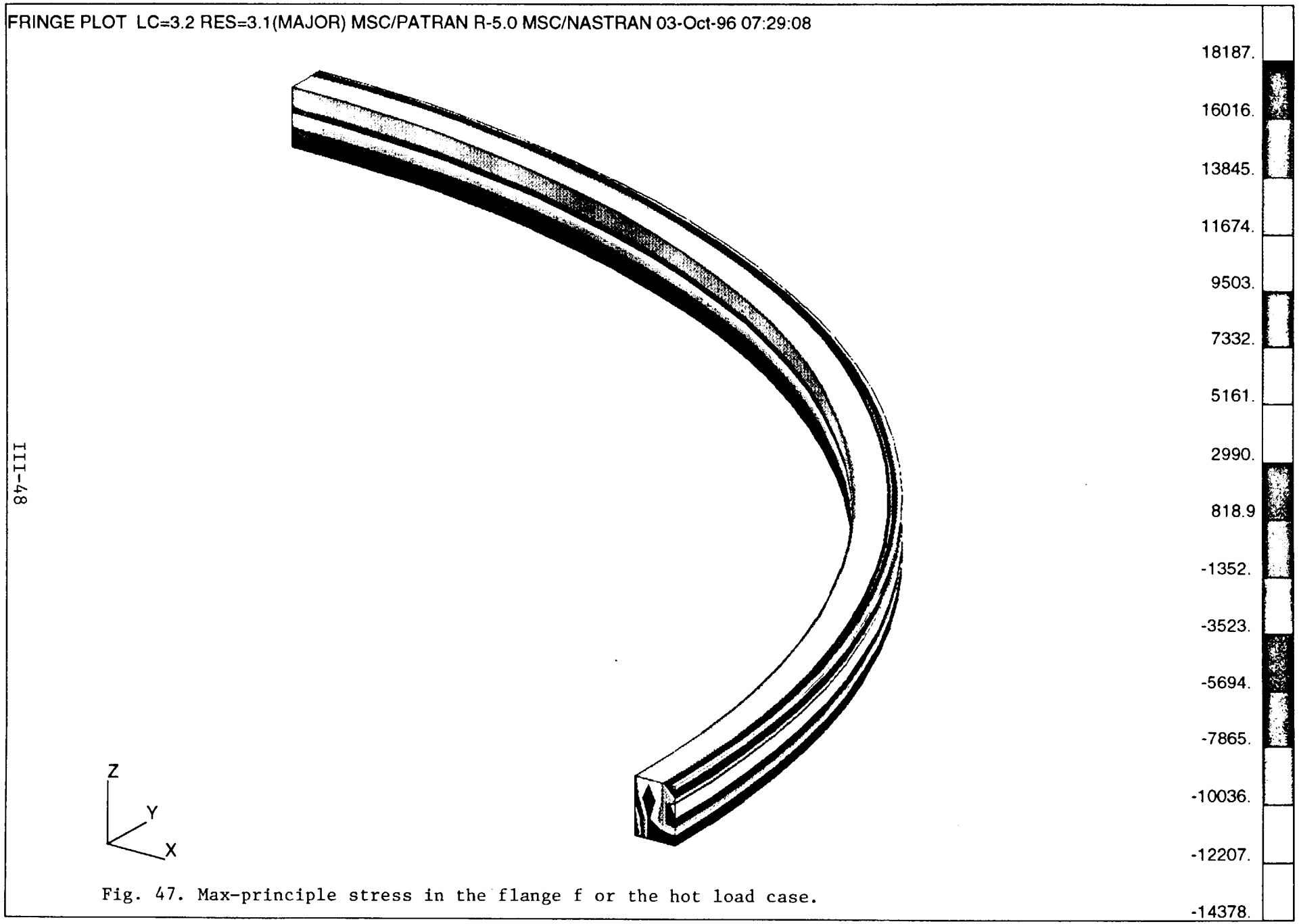

Fig. 47. Max-principle stress in the flange f or the hot load case.

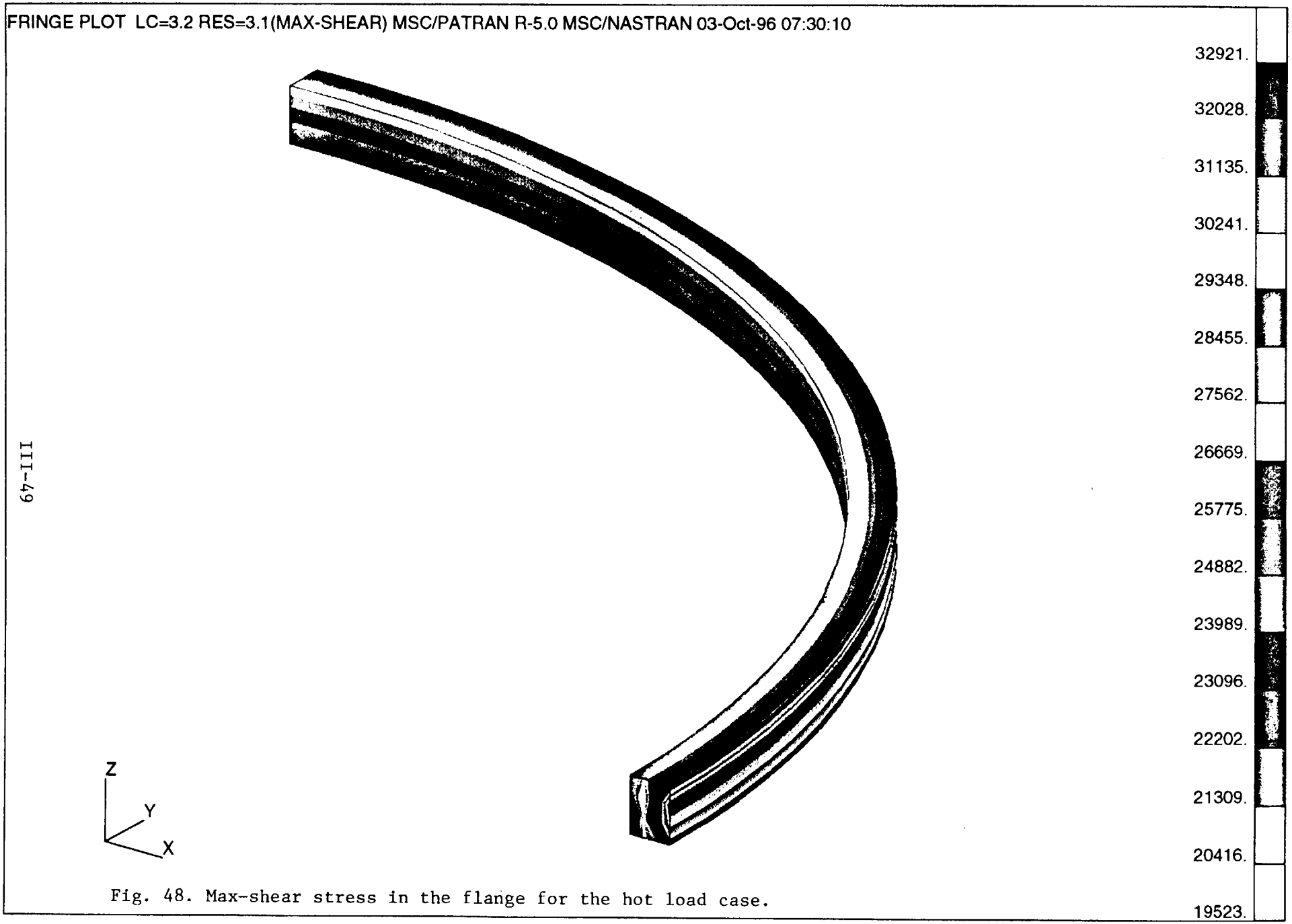

Fig. 48. Max-shear stress in the flange for the hot load case.

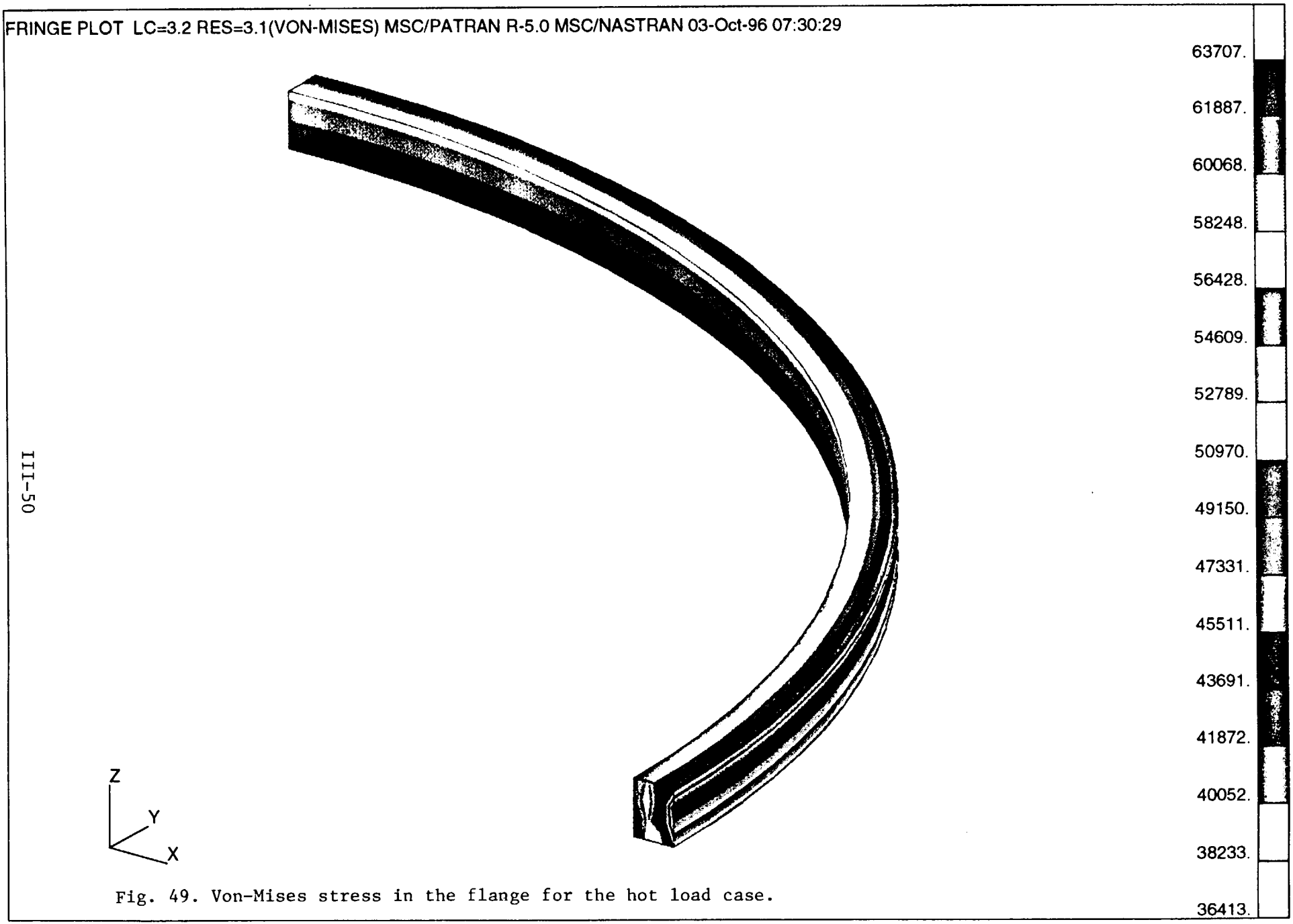

Fig. 49. Von-Mises stress in the flange for the hot load case.